Title

THEORY AND DESIGN PARAMETERS FOR A POSITRON-EMITTER BEAM-IMAGING DEVICE FOR BIOMEDICAL RESEARCH

Author

Llacer, Jorge

Publication Date

1977-05-01

Submitted to Physics in Medicine and Biology

LBL-5631
Preprint c.1

THEORY AND DESIGN PARAMETERS FOR A POSITRON-EMITTER BEAM-IMAGING DEVICE FOR BIOMEDICAL RESEARCH

Jorge Llacer, Aloke Chatterjee, Grant E. Gauger, Cornelius A. Tobias, and Frederick S. Goulding

DONNER LABORATORY

May 1977

Prepared for the U. S. Energy Research and Development Administration under Contract W-7405-ENG-48

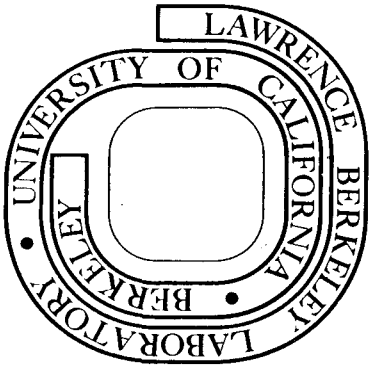

DISCLAIMER

LBL-5631

Theory and Design Parameters for a Positron-emitter Beam-imaging Device for Biomedical Research *

Jorge Llacer, Ph.D., Aloke Chatterjee, Ph.D., Grant E. Gauger, M.D.,†
Cornelius A. Tobias, Ph.D., and Frederick S. Goulding, B.Sc.

Lawrence Berkeley Laboratory, University of California,
Berkeley, California, 94720, U.S.A.

*Work performed under the auspices of the U. S. Energy Research and Development Administration under Contract W-7405-ENG-48.
†Department of Neurological Surgery, University of California, San Francisco, California, 94143

ABSTRACT. The design analysis of an instrument for the imaging of coincidence annihilation gamma rays emitted from the end point of the trajectories of radioactive high-energy heavy ions is carried out. The positron-emitting heavy ions are the result of nuclear fragmentation of accelerated heavy ions used in cancer therapy or diagnostic medicine. The instrument designed will be capable of locating the beam trajectory and points within 1 to 2 mm for an injected activity of 100 nanoCi in a measurement time of 1 sec.

1. Introduction

Charged particles with atomic numbers as high as 18 (Argon) are now being accelerated in a compound accelerator called the Bevalac at the Lawrence Berkeley Laboratory (Grunder 1973). The energies of these particles can be varied to a maximum value of about 3 GeV/nucleon. Because of their very favorable depth-dose characteristics and increased biological efficiency, these particles will be used in radiation therapy (Tobias 1973). In view of this therapeutic goal, many studies are now being directed at the understanding of the biological effects of these heavy charged particles at the cellular and molecular levels.

In addition to therapy, heavy ions are expected to find many useful applications in diagnostic procedures. Already, these particles have been used in radiography for localizing tumors. The results are far better than can be achieved with x rays (Benton, Henke and Tobias 1973).

Although direct acceleration of radioactive particles is not possible in the Bevalac, we have produced a steady flux of radioactive beams through the phenomenon of autoactivation (a physical process in which the projectile particles undergo nuclear fragmentation when they collide with target nuclei). The cross section for the process of autoactivation is large enough to produce such beams with adequate intensities. With the help of proper detection devices, these radioactive particles should allow the development of important new diagnostic procedures hitherto impossible.

At present, we are mostly interested in those fragments that decay by positron emission. These fragments are obtained by the loss of a few nucleons so that they are still heavy enough to exhibit

precise range-energy relationships. Thus, when the beam is directed to a precise location in the body, the initial effect will be the highly localized injection of a positron-emitting isotope at the end of the particle tracks. The annihilation of the positrons generates two detectable 511-keV gamma rays at nearly 180^{o} and in time coincidence. The utilization of this localized initial distribution of positron emitters is of interest both in therapy, as a means to obtain direct information on the location of the region of high cell damage, and in studies related to physiology and nuclear medicine.

Much of the success of this newly proposed usefulness of radioactive beams will depend on the availability of a proper detection device. The purpose of this paper is to present theory and design parameters for a detection device that will image the isotope distribution as a function of time in a target.

2. Basic design constraints

In terms of radiation dose, the injection of a certain amount of activity into a human being by a beam of energetic ions differs considerably from conventional injection into the bloodstream, which does not, in itself, involve any radiation dose. In the case of an ion beam, slowing down of the ions in tissue until they come to rest at the injection point involves a radiation dose that is concentrated principally at the end of the particle tracks. The injection of 0.15 μCi of O^{15}, for example, results in an approximate dose of 1 rad, which could be considered to be the maximum dose for clinical studies. There are approximately 5,500 γ-pairs emitted per second initially as a result of such an injection.

Although the injection dose appears to be a handicap in the successful use of the beam injection technique, activity can be injected by this method into areas of the body where blood flow cannot be studied successfully by other methods as in certain regions of the brain.

One requirement of the imaging instrument that is immediately apparent from the small amounts of activity that can be injected safely is high sensitivity. This requirement can best be met by the use of large crystals of NaI(Tl). Bismuth germanate is not being considered at this time because of its unproven characteristics although its absorbing power is superior to that of NaI(Tl).

In order to bring the detectors as close as possible to the targets, which can range in diameter from approximately 8 to 30 cm, two moving banks of detectors separated by a variable distance are used. For activity confined principally within a cylindrical volume along the axis of the heavy-ion beam trajectory, the detector banks are articulated so that the crystals are aimed approximately toward the beam trajectory line. Figure 1 is a schematic drawing of the conceptual design. Economics dictates the use of standard detector sizes and a limitation to 48 NaI-photomultiplier detectors at this time. 0.75-inch-diameter, 3-inch-long NaI(Tl) detectors (1.91 x 7.62 cm) are used for the two center detectors of each row, and 0.75-inch-diameter, 2-inch-long detectors (1.91 x 5.08 cm) are used for the outer detectors in order to reduce positional ambiguity for gamma rays that interact deep in the detectors. Initial efficiency calculations show that the system will detect approximately 1% of emitted γ-ray pairs in coincidence for a distance

of 10 cm between planes or 22,800 cts/min-μCi, assuming no energy discrimination and no substantial scattering. For a distance of 3 cm between crystal centers, a length of 9 cm along the ion beam axis is covered.

It was also decided that each row of four detectors will constitute a detachable independent module so that the basic instrument can be used in a different or expanded configuration in the future.

The process of image reconstruction from an instrument made with a relatively small number of large detectors requires the development of an appropriate theoretical background.

3. Theory of three-dimensional image reconstruction from a very limited number of projections

The theory discussed here is applicable to cases in which the imaging instrument, constrained by cost and efficiency requirements, consists of a relatively small number of large detectors in some geometric arrangement that spans a volume. In the conventional language of image reconstruction, the detector elements of such systems have large dimensions compared to the desired separation between sampling points, and the number of projections and points per projection that can be obtained from the nonrotating instrument are much too small for a conventional Fourier-based reconstruction algorithm. Another very important characteristic of these systems is that the point response function is not "space invariant" even within a single image plane; that is, moving a point source from $\vec{r}_i$ to $\vec{r}_{i+1}$ does not necessarily form an identical pattern of detector responses displaced at the detector plane by a distance proportional

to $|\vec{r}_i - \vec{r}_{i+1}|$. Under these conditions, solutions to the imaging problem by deconvolution are not feasible. For these very limited systems, we are left then with purely algebraic methods of image reconstruction. The techniques described below not only solve the imaging problem as well as possible but help determine the physical reasons for the limitations of such systems.

4. The system matrix

Let us consider a general array of detectors with n outputs; for example, in a coincidence annihilation radiation detector, there could be n possible chords joining pairs of crystals. If we place a point source during a suitable fixed length of time at position s_j in a set of m source positions, the detectors will respond with a vector of n elements, each element containing the number of times that a detector response has occurred. If this experiment is repeated for all m source positions and the resulting vectors are set side by side as column vectors, we will obtain a system matrix A with n rows (one per possible detector output) and m columns (one for each source position). The m source positions used to obtain the A matrix will be called "system points." With this matrix we can, in principle, solve the imaging problem.

$$A\vec{x} = \vec{k} \tag{1}$$

where $\vec{k}$ is a vector of detector responses caused by unknown amounts of activity $\vec{x}$ placed at the system point s_j. This is an old idea, which was reported by Robertson, Marr, Rosenblum, Radeka and Yamamoto (1973) to lead to considerable error during the inversion process with experimental data in their 32-crystal, positron-annihilation ring detector.

The system of linear equations (Eq. 1) can be solved, however, if care is taken in the choice of system point s_j so that the resulting matrix A behaves well upon inversion in the presence of statistical fluctuations in the experimental vector $\vec{k}$. The fundamental considerations that define the behavior of a matrix upon inversion have been discussed by Wilkinson (1965). Basically, the argument is as follows. A solution to Eq. 1 is equivalent to solving

$$A^T A \vec{x} = A^T \vec{k} \tag{2}$$

where A^T is the transpose of A. Defining $A' = A^T A$ and $\vec{k}' = A^T \vec{k}$, we rewrite Eq. 2 as

$$A' \vec{x} = \vec{k}' \tag{3}$$

where A' is (mxm), and $\vec{x}$ and $\vec{k}'$ are also of dimension m (the number of system points).

From the theory of matrices, we know that A' is symmetric and real and that, for this reason, there exists a transformation H such that

$$H^{-1} A' H = \text{diag}(\lambda_j) = D \tag{4}$$

where D is a matrix with values λ_j in the diagonal elements, the eigenvalues of A', and all other elements zero.

The matrix H of the transformation has columns that form the eigenvectors of A'. In the present case, these eigenvectors $\vec{\chi}_j$ form an orthonormal basis for the space spanned by A' so that the solution $\vec{x}$ to Eq. 3 can be expanded in that basis to

$$\vec{x} = \xi_1 \vec{\chi}_1 + \xi_2 \vec{\chi}_2 + \ldots + \xi_m \vec{\chi}_m \; . \tag{5}$$

Because eigenvectors and eigenvalues are defined by the equation

$$(A' - \lambda_j I)\,\vec{\chi}_j = 0 \tag{6}$$

where I is the identity matrix, it follows from Eqs. 3, 5 and 6 that

$$A'\,\vec{x} = \xi_1\lambda_1\vec{\chi}_1 + \xi_2\lambda_2\vec{\chi}_2 + \ldots + \xi_m\lambda_m\vec{\chi}_m = \vec{k}'. \tag{7}$$

Similarly the experimental result $\vec{k}'$ can be expanded as

$$\vec{k}' = \alpha_1\vec{\chi}_1 + \alpha_2\vec{\chi}_2 + \ldots + \alpha_m\vec{\chi}_m \tag{8}$$

with $\alpha_i = \langle\vec{\chi}_i, \vec{k}'\rangle$, the dot product of the vectors, because of orthogonality of the $\vec{\chi}$'s. Then, equating Eqs. 7 and 8, we can find

$$\xi_i = \frac{\alpha_i}{\lambda_i} \text{ for } 1 \le i \le m, \tag{9}$$

and finally the solution to Eq. 3 is given by

$$\vec{x} = \frac{\alpha_1}{\lambda_1}\vec{\chi}_1 + \frac{\alpha_2}{\lambda_2}\vec{\chi}_2 + \ldots + \frac{\alpha_m}{\lambda_m}\vec{\chi}_m . \tag{10}$$

Because the eigenvectors are all of unit length, it is clear that, in the presence of fluctuations in the experimental results (transmitted to the values of α_i), the resultant vector $\vec{x}$ will be meaningful only if there are no terms in Eq. 10 with values of λ_i that are much smaller than the rest. If this were the case, a small error in the corresponding value of α_i would result in a greatly exaggerated contribution of $\vec{\chi}_i$ to the resulting vector $\vec{x}$.

This result is a fundamental property of the solution. Limitations of the chosen method of solution, truncation errors of the computer, etc., will only aggravate the problem. One simple measure

of the invertibility of a matrix with respect to statistical fluctuations is given by the "condition number" of the matrix,

$$\text{condition number} = \lambda_{max}/\lambda_{min}, \tag{11}$$

which is suitably normalized by the numerator. Evidently, a large condition number is undesirable.

Another very useful concept emerges from the above analysis. Large condition numbers result from a selection of system points in which two or more are too close to each other so that the detector responses do not define the point unambiguously. Large condition numbers also result from system points giving small detector responses because they are hidden from detector view or in the periphery of the field.

In order to illustrate the validity of the above statement, let us consider an imaging system formed by a number of detector rings stacked in the form of a cylinder with system points located at the geometrical center of each ring only as in Figure 2a for a three-ring system. A simple geometrical construction shows that the set of coincidences generated from each system point is totally different from the sets of coincidences from the other points with no coincidences belonging to more than one system point. Under these conditions, matrix A will have a configuration of columns of the form, for example,

$$\begin{pmatrix}
a_{1,1} & 0 & 0 & 0 \\
a_{2,1} & 0 & 0 & 0 \\
a_{3,1} & 0 & 0 & 0 \\
a_{4,1} & 0 & 0 & 0 \\
0 & a_{5,2} & 0 & 0 \\
0 & a_{6,2} & 0 & 0 \\
0 & a_{7,2} & 0 & 0 \\
0 & 0 & a_{8,3} & 0 \\
0 & 0 & a_{9,3} & 0 \\
0 & 0 & a_{10,3} & 0 \\
0 & 0 & a_{11,3} & 0 \\
0 & 0 & a_{12,3} & 0 \\
0 & 0 & 0 & 0 \\
\cdot & \cdot & \cdot & \cdot \\
\cdot & \cdot & \cdot & \cdot \\
\cdot & \cdot & \cdot & \cdot \\
0 & 0 & 0 & a_{m,m}
\end{pmatrix} \qquad (12)$$

The system matrix $A' = A^T A$ will then be purely diagonal with eigenvectors given by unity vectors,

$$\begin{pmatrix} 1 \\ 0 \\ 0 \\ \vdots \\ 0 \end{pmatrix}, \begin{pmatrix} 0 \\ 1 \\ 0 \\ \vdots \\ 0 \end{pmatrix} \quad \cdots \quad \begin{pmatrix} 0 \\ 0 \\ 0 \\ \vdots \\ 1 \end{pmatrix}.$$

The values of the diagonal elements of A' will be the eigenvalues λ_j.

If we consider the eigenvalues λ_j in some detail, we notice that their magnitudes are equal to the sum of the squares of the number of occurrences of all possible coincidences for a particular system point; that is,

$$\lambda_j = \Sigma_i' \, (a_{ij})^2 \, . \qquad (13)$$

This equation indicates that, if one of the system points is only seen by detectors with small efficiency or by fewer detectors,

the eigenvalue corresponding to that point will be smaller than those of the others and lead to a large condition number $\lambda_{max}/\lambda_{min}$.

In a more general case with system points located arbitrarily, matrix A will contain rows that are often not zero in several columns so that A' will not be purely diagonal. It can be diagonalized, however, by a matrix H of eigenvectors (Eq. 4) so that the eigenvalues λ_j appear at the diagonal of $H^{-1}A'H$.

The diagonalization of A' by the matrix H is equivalent to a transformation of the detector system so that there should be, at least in concept, one "ideal" configuration of detectors for any arbitrary set of system points that yields a purely diagonal A' matrix with elements λ_j. If the condition number of this more general system is large, by analogy with the simple case given above the detector locations of the conceptual "ideal" system are so that one or more of the system points are seen very little; that is, few coincidences are seen from that point by the detectors. It is quite clear that this situation will arise when a system point is chosen at a position that results in a poor detector response in the real physical system.

Although less obvious, a large condition number will also occur when one system point is located too near another point so that the column vectors of their responses in the A matrix are not very different. This effect can be readily understood for a very simple case by returning to the example of the stacked rings of detectors with system points at the center of the ring planes only as in Fig. 2. The addition of one more system point on the axis of the cylinder very near one of the "good" system points

will result in A' not being purely diagonal. The diagonalization procedure through H will be equivalent to forming a new "ideal" detector system with one more ring as shown in Fig. 2b. The requirement of the uniqueness of the coincidences forces ring 2' to be much smaller than the others and a reduction in the size of ring 2 as well. System point 2 will have coincidences between rings 2 and 2', but point 2' will have none between the same rings. It is evident that the "ideal" system of Fig. 2b will have a larger condition number than that of Fig. 2a and that the closer point 2' is made to 2, the worse the situation will be.

4. Design analysis of the positron beam-imaging device

The imaging objectives of the design shown in Fig. 1 can be summarized as follows:

(i) ability to locate a point source on the ion-beam axis with an activity of 0.1 to 0.2 μCi with an accuracy on the order of 1 to 2 mm in a counting time of a few seconds;

(ii) ability to observe quantitatively the disappearance rate of activity from the injection point on the ion-beam axis; and

(iii) ability to obtain the best possible quantitative information on activity as a function of time in the volume spanned by the detector planes consistent with the limited number of projections available.

The first two objectives involve finding the optimum relative positions in the x direction (Fig. 1) of the twelve detector modules of banks A and B (four detectors per module) so that system points on the

center axis can be located very near each other and still result in a well behaved matrix. The second objective requires the investigation of matrices obtained from three-dimensional arrays of points. For practicality in data presentation and interpretation, the array should be rectangular.

4.1 Eigenvalue analysis

System matrices to simulate the physical system have been obtained by digital calculations; the two arrays of 24 detectors have been simulated with their actual dimensions in space. For a particular point source at s_j, the projections from a raster of points at the entrance surface of every detector of bank A, passing through s_j and intersecting entrance surfaces of detectors of bank B, have been calculated. For all lines passing through s_j that join two opposite detectors, the length of the γ-ray trajectories inside the cylindrical detectors and the corresponding probabilities of interaction have been obtained (photoelectric plus Compton). From these probabilities it is possible to construct a column vector of 576 elements (24 x 24) that contains as entries the frequencies with which all possible coincidences from s_j can occur. Repeating the procedure for all system points under investigation and placing the column vectors side by side, we obtain the system matrix A. Multiplicaiton by A^T yields the symmetric matrix A', which can then be analyzed in terms of the eigenvalues. The simulated system should be a good representation of the physical system. The only physical phenomenon not included is the interaction in a crystal of photons that do not enter through the entrance window of the same detector crystal. The consequences of this simplification will be discussed below. Interaction in more than one crystal

of the same bank in time coincidence will be rejected electronically so that they need not be of concern in the simulation.

4.1.1 System points on axis only

The simplest configuration of detectors to be tested is one in which the columns of detectors are vertical and the detectors in banks A and B are in direct opposition. Figure 3 shows the location of the detectors in the (y,z) plane as defined in Fig. 1 for a distance of 10 cm between detector banks. The lines shown correspond to the axes of the cylindrical NaI detector with the innermost ends of each line at the entrance faces. Figure 4 shows the projection on the (x,y) plane of the centers of the detector faces. Detectors of banks A and B are shown with + and x marks, respectively. The location of a system of four points, each one at the center of two directly opposing detector columns, is shown by circles in Fig. 4. Figure 5a shows the magnitude of the elements constituting the (4x4) symmetric matrix A' plotted by columns, and Fig. 5b shows the normalized eigenvalues and the condition number as the ratio $\lambda_{max}/\lambda_{min}$.

Reducing the distance between sampling points by a factor of 2, i.e., placing the system points at a distance from each other equal to the sampling distance of the center line by the array, gives the results of Fig. 6, still with a very low condition number. Attempts to reduce the inter-point distance further lead to extremely high condition numbers as seen in Fig. 7.

In order to increase the sampling frequency at the center line, the arrangement of Fig. 8 has been devised. By displacing contiguous rows of detectors in a given plane by 0.5 cm and using

a crossed pattern between banks A and B, a simple geometrical construction shows that the center axis is now sampled every 0.5 cm. Figure 9 shows the condition number of the matrices generated in this arrangement as a function of Δx, the inter-point distance. Only the central 5 cm of the axis are being sampled in this study. The fast rise in $\lambda_{max}/\lambda_{min}$ for $\Delta x < 0.7$ cm is, undoubtedly, due to ambiquity in the column vectors of contiguous points caused by the large dimensions of the crystals. The well behaved system that will be studied further in this analysis will be the one labeled S-1 in Table 1, in which NX, NY and NZ correspond to the numbers of system points in each direction and ΔX, ΔY and ΔZ are the distances between points. S-1 is shown in the (X,Y) plane in Fig. 8.

4.1.2 System points in the spanned volume

A preliminary analysis of condition numbers for a three-dimensional system shows that the irregular geometry of the detector array results in optimal system points located irregularly in space. At the expense of some loss in invertibility, a rectangular mesh of points will be sought. Attempts to locate points in the (y,z) plane at distances less than 1.75 cm from the center axis result in very high condition numbers. Indeed, there are very few crossings of lines connecting detector centers of opposite banks in a graph like that of Fig. 3 at distances less than 1.75 cm from the center; that is, the sampling rate in the (y,z) plane is quite low in all orientations.

For the purposes of the design analysis, four fairly well behaved systems will be studied. They are characterized in Table 1 (Systems S-2 through S-5). S-2 is shown in the (x,y) plane in

Fig. 10, and S-4 is shown in the (y,z) plane in Fig. 11. All systems in Table 1 are for a 10-cm separation between detector banks.

4.2 Imaging Capabilities

To establish the imaging capabilities of the systems of Table 1, a set of sources of variable strength has been simulated in the computer. The response of the chosen detector configuration is given by vector $\vec{k}$ of Eq. 1. Premultiplication of $\vec{k}$ by A^T for the system under test yields $\vec{k}'$ of Eq. 3. The equation can then be solved for $\vec{x}$, and the results can be displayed conveniently.

In the computer simulation, vector $\vec{k}'$ contains the statistical fluctuations corresponding to the actual source strength introduced into the results individually for each possible coincidence. Matrix A is assumed to be essentially free of fluctuations because it can be obtained in a physical system with strong sources and/or long count times. Solutions to Eq. 3 have been carried out by the conjugate gradient method as described by Beckman (1960), which is guaranteed to arrive at the best solution in the least-squares sense. Calculations have been carried out in single-precision, floating-point arithmetic (32 bits) in a PDP 11/45 computer.

Displays have been generated by using the sampling theorem in three dimensions. The solutions for the source position and strength are known only at the system points. Because of the Nyquist sampling theorem, it is clear that the best estimate that we can make about the true source is given by the expression

$$f(x,y,z) = \sum_{i,j,k} g(i,j,k)\,\mathrm{sinc}\left(\frac{x}{\Delta x} - i\right)\mathrm{sinc}\left(\frac{y}{\Delta y} - j\right)\mathrm{sinc}\left(\frac{z}{\Delta z} - k\right) \qquad (14)$$

where sinc(x) = sin(πx)/(πx), i,j,k are sampling point indices (system points), g is the solution known at the system points and f is the estimated function. The indices i,j,k are zero at x,y,z equal to zero. In order to avoid some of the "ringing" associated with Eq. 14, a guassian weighting function has been used to dampen the tails of the sinc functions. Negative values of g have been set to zero because they have no physical meaning.

The generated displays contain on the left a description of the source to be imaged, composed of one or more discrete points. The source strength of a point is represented by the size of the rhombus at its position. The image of the source on the right of the display presents a continuous appearance because of Eq. 14. The level of activity is represented by the density of data per unit volume in the represented space. Density levels have been chosen so that level 32 corresponds to 1 μCi or 0.1 μCi of activity at a system point (low- and high-sensitivity displays). Results below level 1 are not plotted. Count time is assumed to be 1 sec for all simulation experiments. Large count times are equivalent to a proportional increase in source strength.

4.2.1 System points on axis only

Figures 12 a through d show the images of point sources located at the centers of the systems with activities of 1,000, 500, 200 and 100 nanoCi imaged during 1 sec in the simulation. The display sensitivity is 1,000 nanoCi. System S-1 of Table 1 was used for the simulations. The images generated for the present case of

a source point at the location of a system point show a density distribution of 0.8 cm FWHM, a peak position error smaller than 0.05 cm and errors in the detected activity ranging from approximately 5% for 1,000-nanoCi sources to 25% for 100-nanoCi sources.

Figures 13 a through d show images of 100-nanoCi sources at x = 0, 0.25, 0.50 and 0.75 cm from the center. The display sensitivity is 100 nanoCi. The images at x = 0.25 and x = 0.50 correspond to point sources not located at system points. It can be proven that, if a detector system results in vectors $\vec{k}$ for such points that are a linear combination of the column vectors corresponding to the surrounding system points, it is possible to find the location and activity of the true source point from the solution at the surrounding system points. If the results vector $\vec{k}$ for point sources not located at system points is not a linear combination of the surrounding system point vectors, there is no a priori knowledge of what the result of solving Eq. 1 might be. The present model of the system under study does not fulfill this "linearity" condition well because a small motion of the source can result in the complete appearance or disappearance of one or more coincidences. If the system points are brought closer together, the above "linearity" condition will be increasingly valid although the condition number of the matrix will become worse. It follows that attempts to improve localization (i.e., the ability to find the true position of a source) and performance under statistical fluctuations will be contradictory. In a real physical system with gamma rays entering the crystals from points other than the entrance windows, through lead shielding, for example, the above "linearity" condition should

improve although for the same reason condition numbers will be somewhat worse than at present. A compromise system-point separation must be adopted.

The broadening in Figs. 13 b and c due to two system points' contributions to the displays at x = 0.25 and 0.50 cm is quite evident. The centroids of the density distributions are, however, within less than 2 mm from the correct source positions with FWHM ranging from 0.95 to 1.4 cm. Detected activity is within 25% of the correct value for the 100-nanoCi sources at a 1-sec count time.

The presence of side lobes of activity clearly seen in Fig. 13e is typical of the solution of Eq. 1 and becomes stronger when the condition number of the matrix increases. This effect is independent of the chosen method of solution, and it appears strongly for source points not on system-point locations.

The behavior of the on-axis system when activity is off-axis is shown in Figs. 14 a through d. In each case, the point source is displaced 0.25 cm farther from the center in all three directions. X information is fairly well preserved. Detected activity decays at a rate roughly proportional to 1/d where d is the shortest distance to the center line.

Figures 15 a through d show the ability of the system to separate two point sources with an activity ratio of 10. The disappearance of the 100-nanoCi source in Fig. 15d is due to a negative lobe at x = 0 in the solution for the hotter source. Finally, the ability to distinguish a "cool" section in a line is shown in Figs. 16 a through d. The ratio of activities is 5:1. A "cool" section of 0.6 to 0.8 cm is distinguishable with an activity of 500 nanoCi per cm in the hot part for a count time of 1 sec.

From the above simulation, we feel that the performance objective of the system along the center ion-beam line has been met successfully. The time required for the iterative solution routine in a PDP 11/45 computer is approximately 0.3 sec for the on-axis case.

4.2.2 System points in the spanned volume

A direct comparison of imaging characteristics of systems S-2 and S-3 of Table 1 for point sources in shown in Figs. 17 and 18. The two systems have the same number of system points, but they differ in Δx, the separation between planes in the direction of the heavy-ion beam (1 cm and 0.75 cm, respectively). Figures 17 a through e correspond to 1,000-nanoCi point sources at x = 0, 0.25, 0.50, 0.75 and 1 cm for system S-2; Figs. 17 f through j are the corresponding images generated by system S-3. Figs. 17 a, e, f and i are for sources at system points. The images presented are quite wide in the (y,z) plane as expected from a sampling distance of 2 cm in that plane. Definition along the x axis is, however, comparable to the results presented above for system points along the x axis only.

Inspection of the two groups of results shows that system S-3 delivers better images than system S-2 for source points not on system points. For these high-activity cases, when statistics are not a principal limitation, fewer artifacts appear in the image when system planes are closer in the x direction. The "linearity" condition discussed in the previous section is better fulfilled for S-3 than for S-2.

Figures 18 a through j show results for a set of images equivalent to those of Fig. 17 but for 100-nanoCi source points. Results

for most point sources show poor localization, and the advantage of S-3 over S-2 obtained for the higher activity has now disappeared. The higher condition number of S-3 evidently eliminates its better "linearity" characteristics in the presence of strong statistical fluctuations. It must be pointed out that the differences in every pair of images for S-2 and S-3 from the same source position and activity are only due to the invertibility characteristics of the A matrices because the sequences of random numbers used to generate the statistical fluctuations have been made identical.

The behavior of S-2 for a point source moving diagonally in three dimensions between the two system points at (x,y,z) = (0,0,0) and (2,2,2) cm is shown in Figs. 19 a through h for 1,000 nanoCi of activity. The appearance of artifacts and the diffusion of the source are quite apparent near the middle of the trajectory when system points are far from the source. These effects are due to lack of "linearity" as defined above.

The comparative behavior of S-4 and S-5 for central point sources of 1,000 and 100 nanoCi is shown in Figs. 20 a through d. Both systems exhibit poor localization, but results are worse in the case of S-5 owing to a high condition number in the system matrix. Solution times for 63 system points range between 2 and 4 sec in the PDP 11/45 computer.

The possibility of using sequential subsystems of S-2 consisting of 3 x 3 points in planes perpendicular to the x axis or 7 x 3 points parallel to the x axis has been investigated. Solutions one plane at a time are successfully used by Chang (1976) and by Perez-Mendez, Chang and MacDonald (1976) in a deconvolution process.

The matrices obtained in our case have very low condition numbers, but the results of inversion of the subsystems are not better and are often much worse than the results obtained with the complete system because of the following two facts:

(i) errors in the system solutions are due to the basic physical limitations of the instrument and not to the mathematical process used in the solution;

(ii) decoupling one plane of points from another by the use of subsystems destroys the nearly "linear" relationship between contiguous planes. With separate subsystems, activity positioned between two planes appears at full strength in both subsystem solutions instead of being "shared" as happens with the complete system.

It follows that, for the instrument being studied, complete matrices for points spanning the volume are needed.

The above analysis is valid for a 10-cm distance between detector planes. At the higher separation of 30 cm, the following results are obtained:

(i) sensitivity in total number of coincidences per unit activity and time decreases by roughly a factor of 3; a substantial decrease in subtended solid angle is partly offset by the gamma rays entering the detectors more parallel to their cylindrical walls, increasing the interaction probability;

(ii) the condition number of systems on the central axis only are very similar to the ones obtained at a 10-cm distance;

(iii) condition numbers for systems occupying the volume between

planes are higher than those at 10 cm by a factor of approximately 2 unless the separation Δz (Fig. 11) is increased 50 to 100%.

From these observations, it appears that the characteristics of the instrument at the higher separations between planes will still be within the initial design specifications.

5. Electronic characteristics

The detailed characteristics of the electronic design will be the subject of a later paper. From the point of view of the present design analysis, it is important to describe the expected coincidence time resolution as it affects the imaging characteristics. For a distance between planes of 10 cm, the computer calculations give a rate of coincidence events $C_o = 390\ (\text{sec-}\mu\text{Ci})^{-1}$ for a point source at the geometric center of the system. The singles rate in one bank of detectors is $C_s = 1{,}195\ (\text{sec-}\mu\text{Ci})^{-1}$.

The accidental coincidence rate is given by $C_s^2\,\Delta t$ where Δt is the coincidence resolving time. The NaI-crystal-photomultiplier combination and the circuits developed for this instrument will allow a value of $\Delta t \simeq 30 \times 10^{-9}$ sec FWHM for the complete system. Even with 100 μCi between the planes, the accidental coincidence rate is approximately 1.1% so that no problems are expected due to accidentals in any of the operating modes comtemplated for the instrument. The excellent coincidence resolving time is also a safeguard against image deterioration by other kinds of radiation in the experimental environment.

The computer simulations discussed above assume no energy discrimination. The instrument will have a very flexible capability

in this respect by the use of a microprocessor for energy window selection with automatic calibration of all 48 photomultiplier tubes. The microprocessor will also assist in interfacing with the PDP 11/45 computer where real-time imaging will be carried out.

The generation of the system matrices in the physical instrument will be carried out automatically under computer control by the use of a source positioner with motion in three dimensions. A 20-μCi point source embedded in plastic can give one column of the system matrix A for one system point in a few seconds.

Absorption effects can be dealt with by generating the system matrices with the point source moving inside a water container of appropriate geometry. High-density absorbing regions simulate the anatomical characteristics of the region to be observed. Effects due to positron range before annihilation in tissue, which make the images less precise than in the case of point sources, can also be incorporated in the system matrices by this procedure.

Preliminary measurements with a detector system designed as described above have already been carried out, and our findings support the essential correctness of the computer simulations.

6. Conclusions

The theory and design analysis discussed above support the possibility of constructing an instrument for imaging very small amounts of positron-emitting radioactivity in heavy-ion injection from an accelerator. The required high sensitivity is obtained with relatively large NaI crystals, and accurate position information

along the beam line is obtained by correct positioning of the crystals in the arrays. The instrument will not only allow the initiation of physiological studies heretofore impossible but will be of great assistance in the on-line visualization of the region of high cellular damage during heavy-ion cancer treatment. The concepts developed are of immediate use in the design of a more complete instrument for the rapid imaging of a volume in finer detail in planes perpendicular to the beam axis than has been possible with the present limited design.

7. Acknowledgements

The authors wish to acknowledge the strong support of Dr. E. L. Alpen in all phases of the project.

SUMMARY

The use of high-energy heavy ions in radiography, cancer therapy, physiological studies and diagnostic medicine is being implemented at the Lawrence Berkeley Laboratory. In particular, the use of positron-emitting isotopes generated by nuclear fragmentation from an accelerated beam allows the injection of known amounts of activity into highly localized volumes of the body. Studies based on this beam injection technique require the design of a very sensitive instrument to image the isotope distribution with high positional accuracy. This paper describes the design of a 48-crystal imaging device that will be able to locate the end point of an ion beam trajectory within 1 to 2 mm for an injected activity of 100 nanoCi in a measurement time of 1 second. System design has been carried out by computer simulation and eigenvalue analysis. It is shown that the use of NaI crystals of relatively large dimensions (1.91 cm diameter) for efficient detection of the 511-keV coincidence gamma rays still allows designing a system that samples the center line of the beam axis every 0.75 cm with a resulting set of equations whose solution is quite immune to the statistical fluctuations resulting from the measurement indicated above. Computer simulation of the imaging characteristic of the instrument designed is investigated for a variety of situations, and calibration procedures for the instrument are described.

REFERENCES

BECKMAN, F. S., 1960, in Mathematical Methods for Digital Computers, (New York: Wiley.)

BENTON, E. V., HENKE, R. P., and TOBIAS, C. A., 1973, Lawrence Berkeley Laboratory Report LBL-2016.

CHANG, L. T., 1976, LBL-4887.

GRUNDER, H. A., 1973, LBL-2090.

PEREZ-MENDEZ, V., CHANG, L. T., and MACDONALD, B., 1976, in Proceedings of 1st Asia & Oceania Congress of Nuclear Medicine.

ROBERTSON, J. S., MARR, R. B., ROSENBLUM, M., RADEKA, V., and YAMAMOTO, Y. L., 1973, in Tomographic Imaging in Nuclear Medicine, (New York: Society of Nuclear Medicine, Inc.)

TOBIAS, C. A., 1973, Radiology, 108, 145.

WILKINSON, J. H., 1965, The Algebraic Eigenvalue Problem, (Oxford: Clarendon Press.)

Table 1

System	NX	ΔX	NY	NZ	ΔY = ΔZ	Cond. No.
S-1	11	0.75 cm	-	-	-	4.36
S-2	7	1.0 cm	3	3	2 cm	20.9
S-3	7	0.75 cm	3	3	2 cm	74.1
S-4	4	1.0 cm	5	3	2 cm	38.6
S-5	4	1.0 cm	5	3	1.75 cm	139.1

FIGURE CAPTIONS

Fig. 1. Schematic drawing of the positron-emitter, beam-imaging system showing the detector entrance faces of one of the banks. The ion-beam direction is given by the center line, the x axis.

Fig. 2. (a) Cross section of a hypothetical system consisting of three detector rings and three system points in the respective centers, resulting in a purely diagonal system matrix A'. (b) Four-ring structure required for a purely diagonal system matrix A' when a new point 7' is added to the above.

Fig. 3. Schematic drawing of the (y,z) plane of the detector system. Lines are center axes of the cylindrical NaI detectors. The distance between planes is 10 cm.

Fig. 4. Projection on the (x,y) plane of the NaI-crystal entrance-face centers for detector banks A and B. A vertical column system is shown here with four system points; $\Delta x = 3$ cm.

Fig. 5. (a) Representation of the normalized values of the elements of the symmetric system matrix A' plotted one column at a time for the four-point system of Fig. 4. (b) Normalized eigenvalues for the same system showing "condition number."

Fig. 6. Same as Fig. 5 except the system now consists of seven points; $\Delta x = 1.5$ cm.

Fig. 7. Effect of Δx smaller than the sampling distance with a very high condition number.

Fig. 8. Projection on the (x,y) plane of the criss-cross detector pattern that results in a sampling distance of 0.5 cm for the center axis. Location of system points for S-1 of Table 1.

Fig. 9. Condition numbers for system matrices as a function of Δx for imaging of the central axis only.

Fig. 10. Projection on the (x,y) plane of system S-2, Table 1.

Fig. 11. Projection on the (y,z) plane of system S-4, Table 1.

Fig. 12. Images created by S-1 for a source of decreasing strength (in nanoCi) at the center of the system. Count time = 1 sec; low-sensitivity reconstruction.

Fig. 13. Images created by S-1 for a low-strength source moving along the x axis. Count time = 1 sec; high sensitivity.

Fig. 14. Images created by S-1 for a high-strength source moving away from the center along the line $x = y = z$. Count time = 1 sec; low sensitivity.

Fig. 15. Images created by S-1 for two sources of 10:1 ratio as a function of position of the hot source. Count time = 1 sec; low sensitivity.

Fig. 16. Images created by S-1 for a line source with a growing "cool" region in the center section. Count time = 1 sec; low sensitivity. A cool spot of 0.6 to 0.8 cm, 5:1 activity ratio, is visible.

Fig. 17. Images created by three-dimensional systems S-2 and S-3 for a point moving along the x axis. High-activity source (1,000 nanoCi); count time = 1 sec; low sensitivity. S-3 images are better in source localization.

Fig. 18. Images similar to those of Fig. 17; low-activity source (100 nanoCi); count time = 1 sec; high sensitivity. S-2 and S-3 images are now both very similar.

Fig. 19. Images created by S-2 for a high-strength source moving away from the center along the line x = y = z. Count time = 1 sec; low sensitivity.

Fig. 20. Comparing images created by S-4 and S-5 from central source, high and low activities. Count time = 1 sec. Both systems show poorer localization than S-2 and S-3 owing to their higher condition numbers. S-5 is markedly worse.

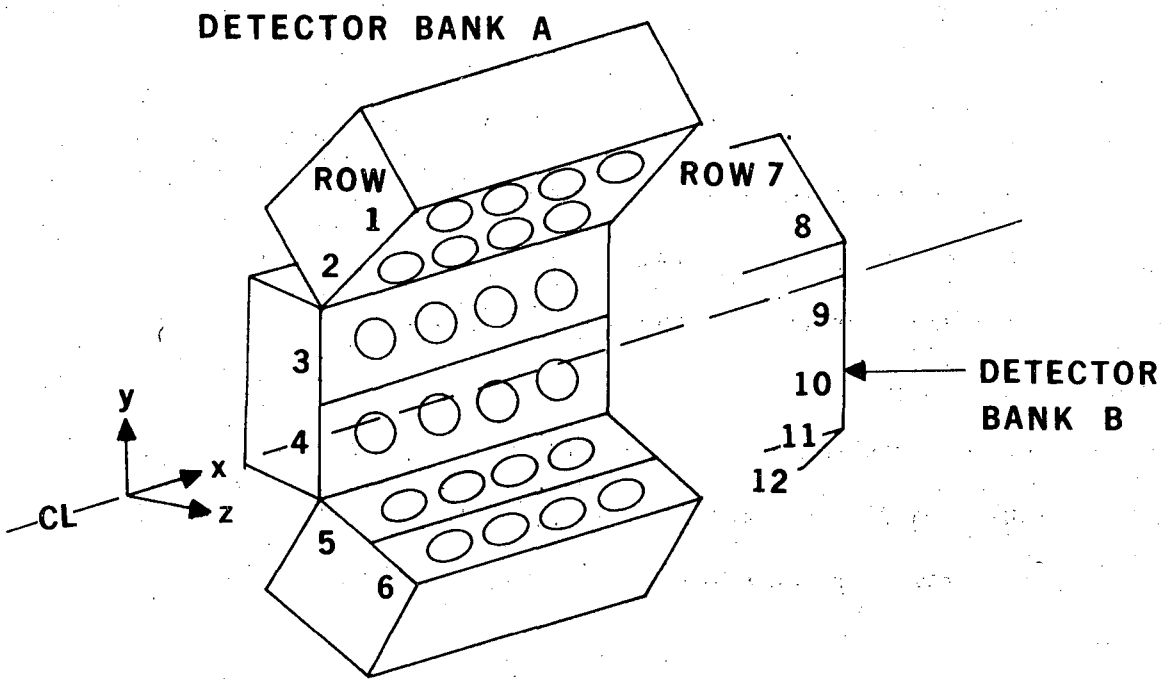
DETECTOR BANK A
ROW 1
ROW 7
2
3
4
5
6
8
9
10
11
12
DETECTOR BANK B
y
x
z
CL
XBL 772-7742

Fig. 1

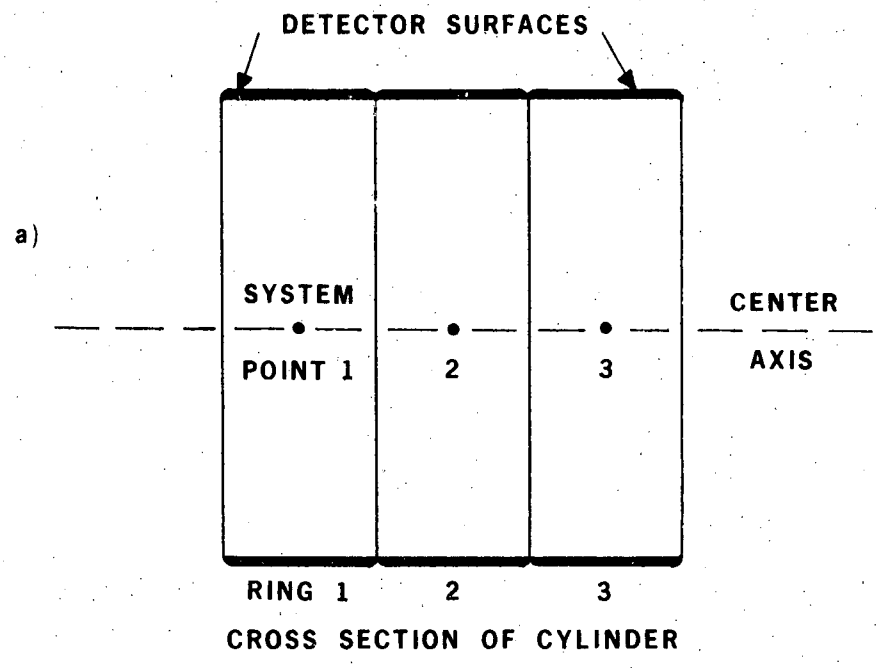

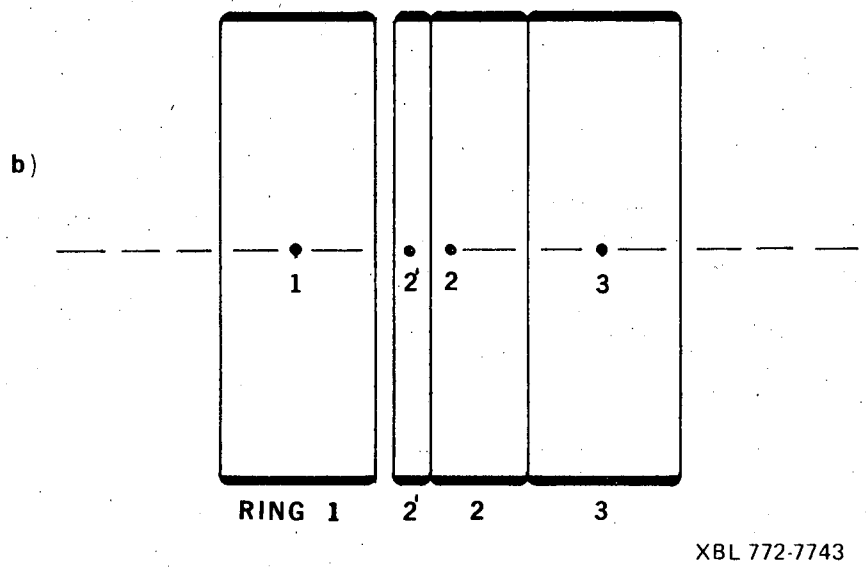

Fig. 2

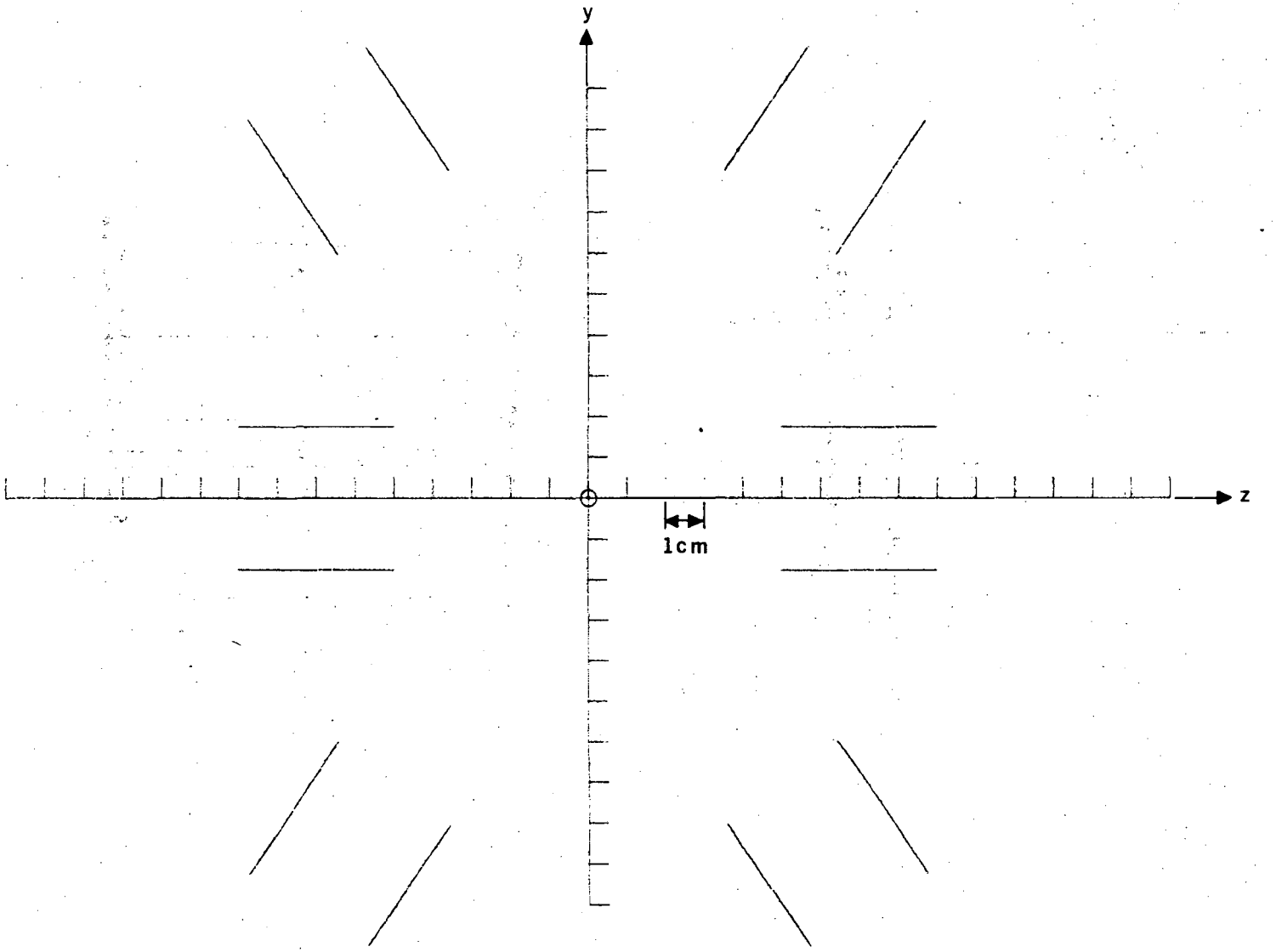

XBL 772-7744

Fig. 3

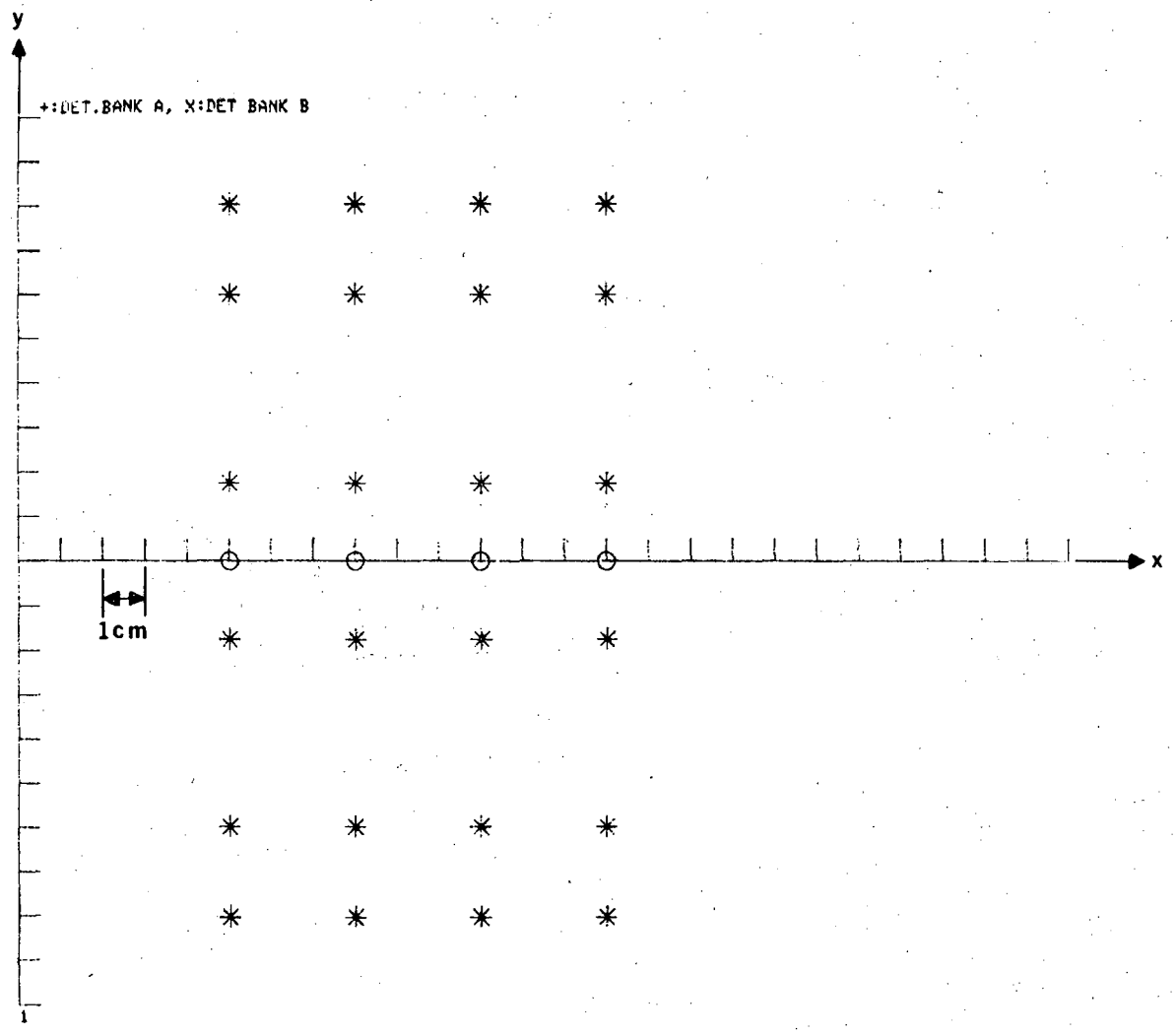

XBL 772-7745

Fig. 4

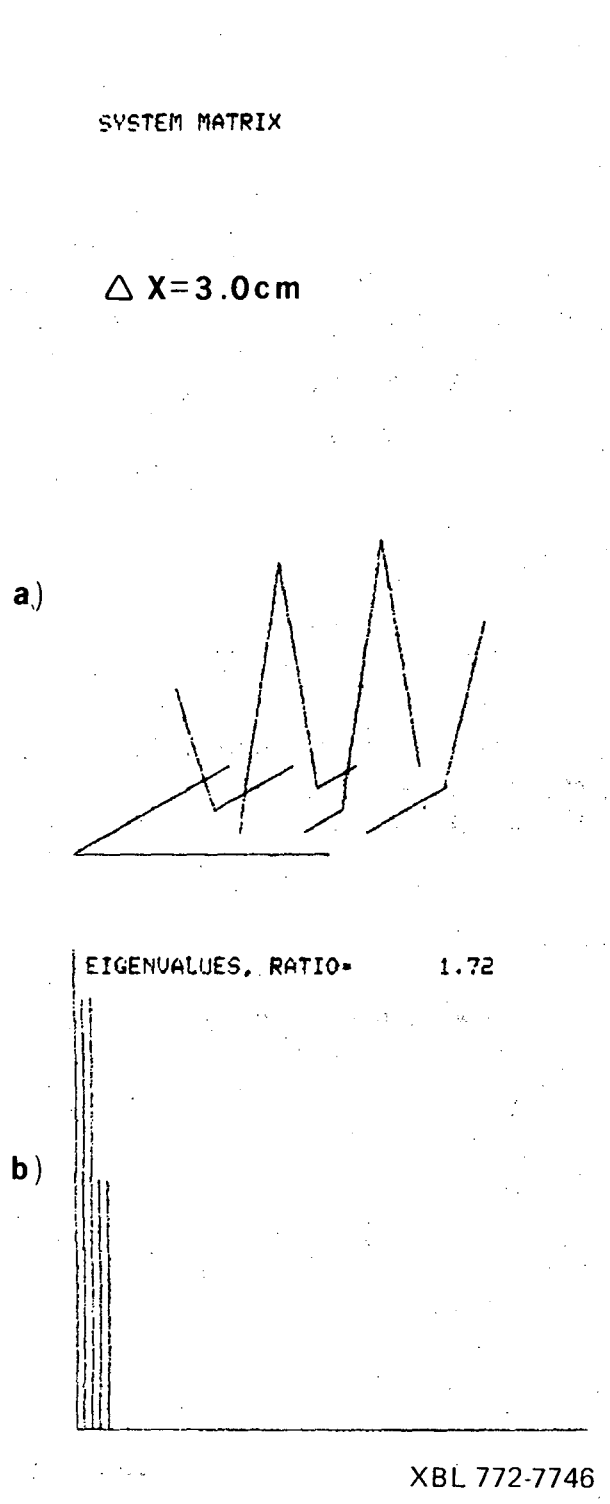

Fig. 5

SYSTEM MATRIX

$\Delta X = 1.5cm$

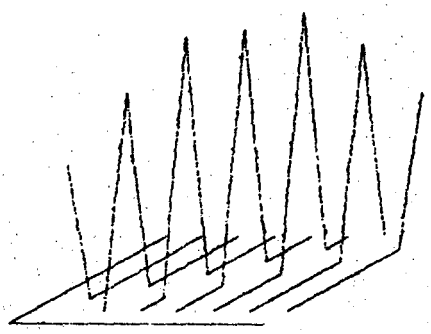

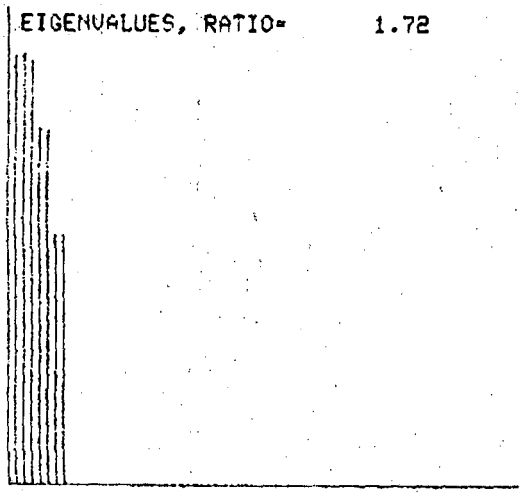

XBL 772-7747

Fig. 6

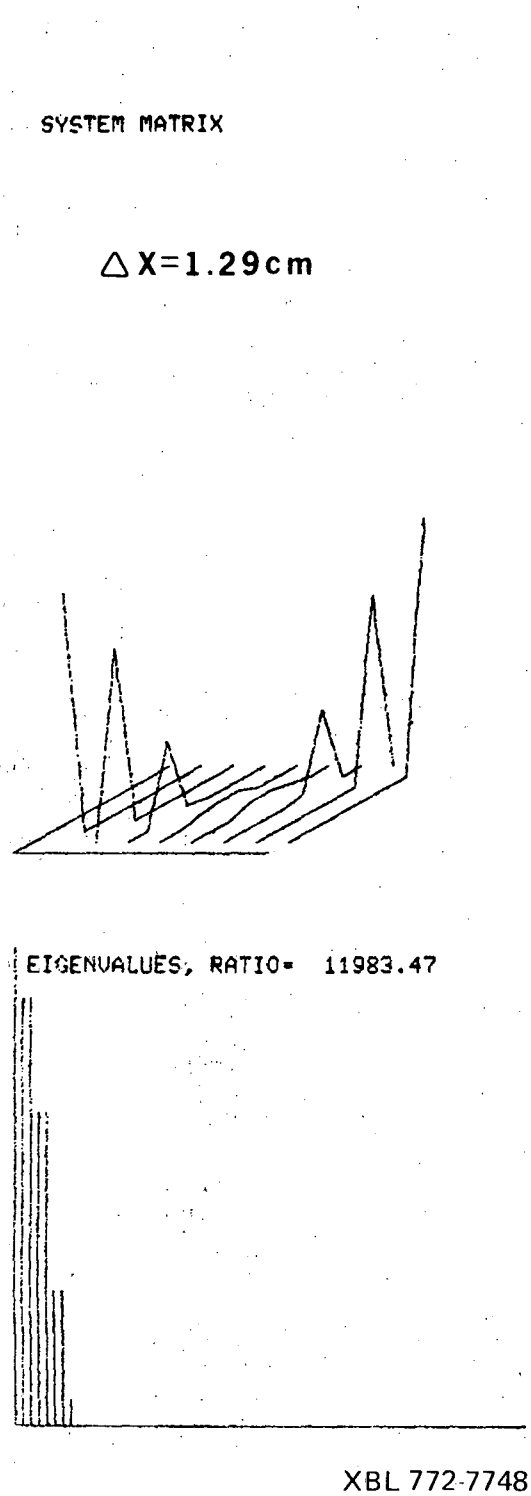
SYSTEM MATRIX
△X=1.29cm
EIGENVALUES, RATIO= 11983.47
XBL 772-7748

Fig. 7

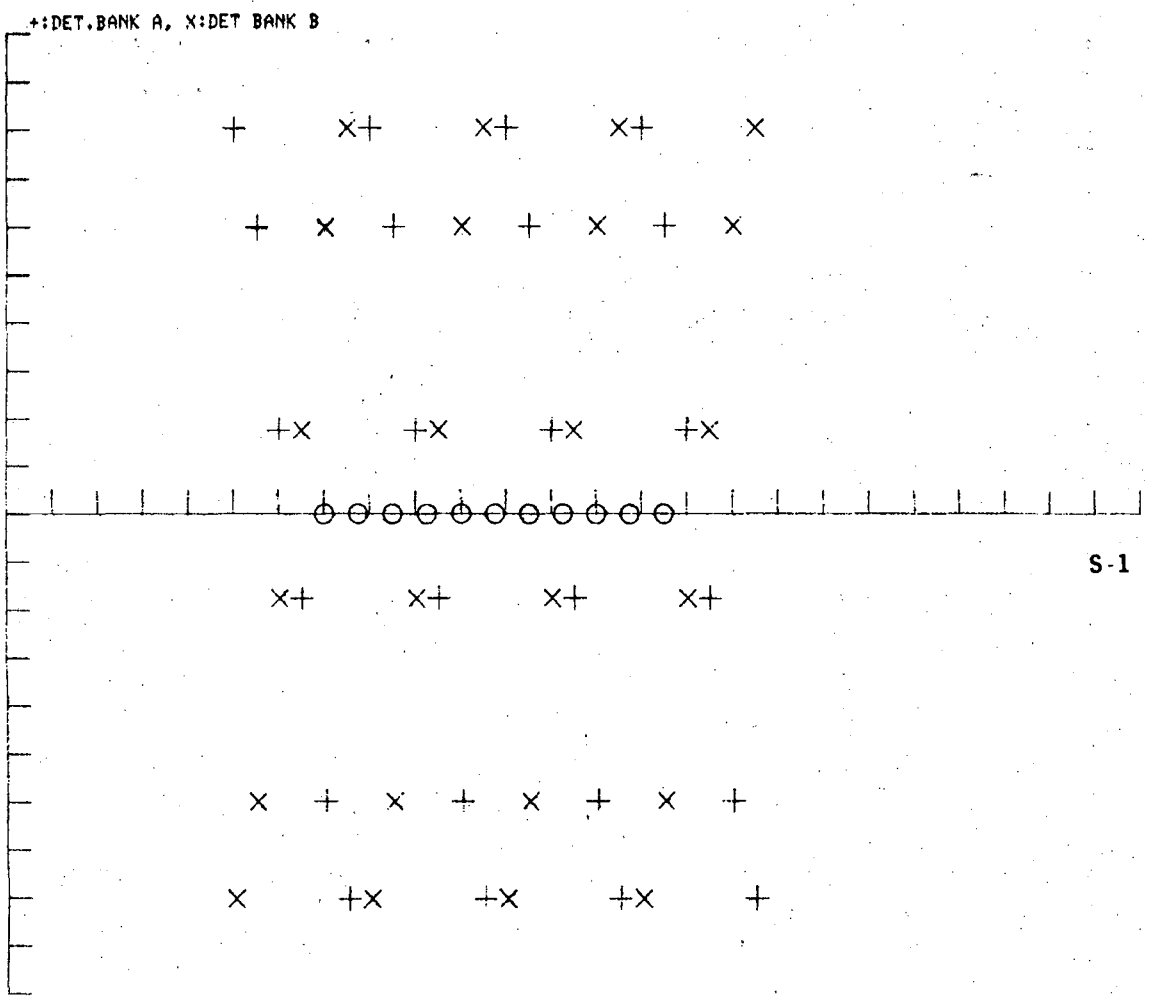

XBL 772-7749

Fig. 8

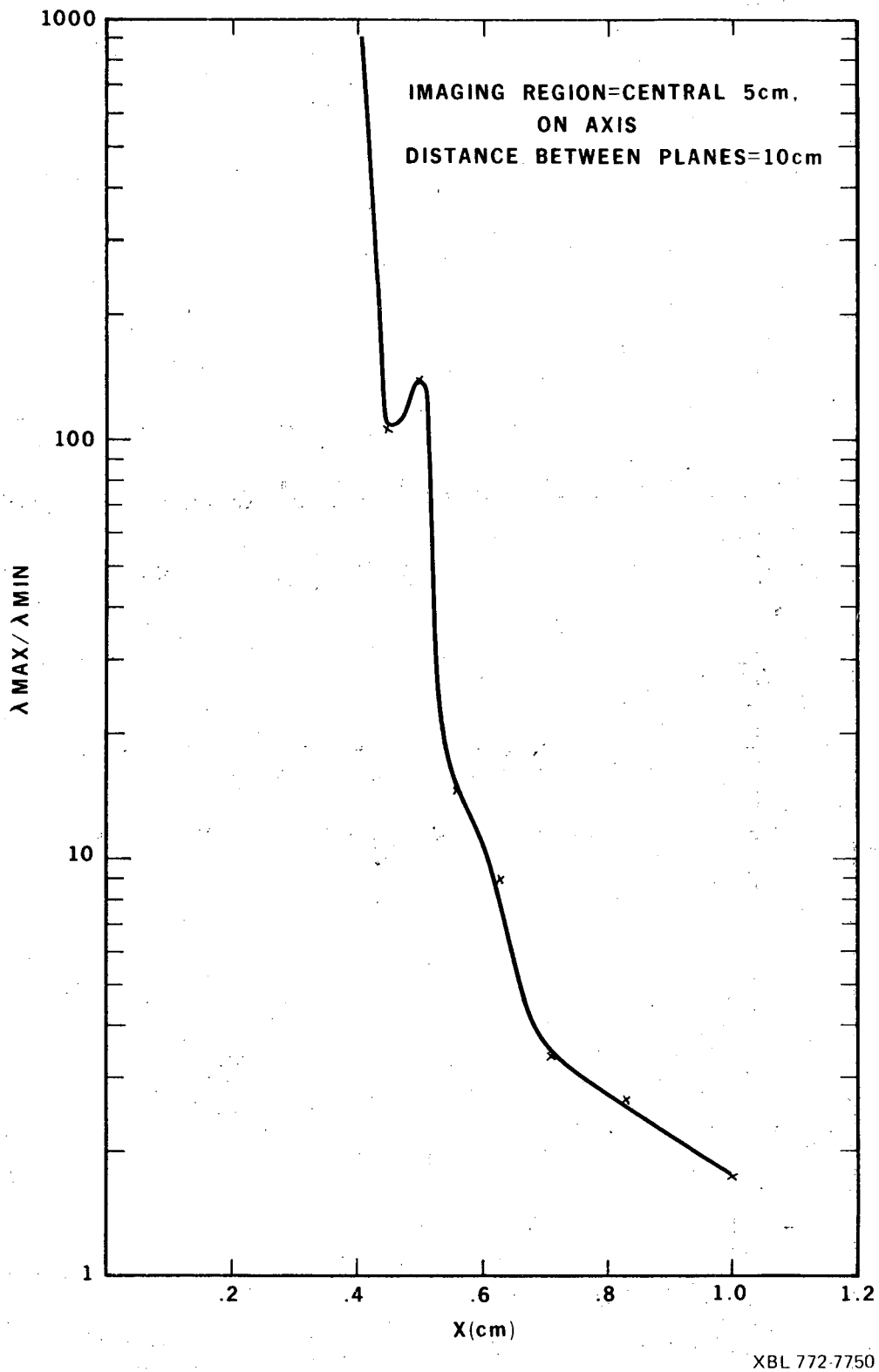
IMAGING REGION=CENTRAL 5cm,
ON AXIS
DISTANCE BETWEEN PLANES=10cm
1000
100
10
1
λ MAX/ λ MIN
.2
.4
.6
.8
1.0
1.2
X(cm)
XBL 772-7750

Fig. 9

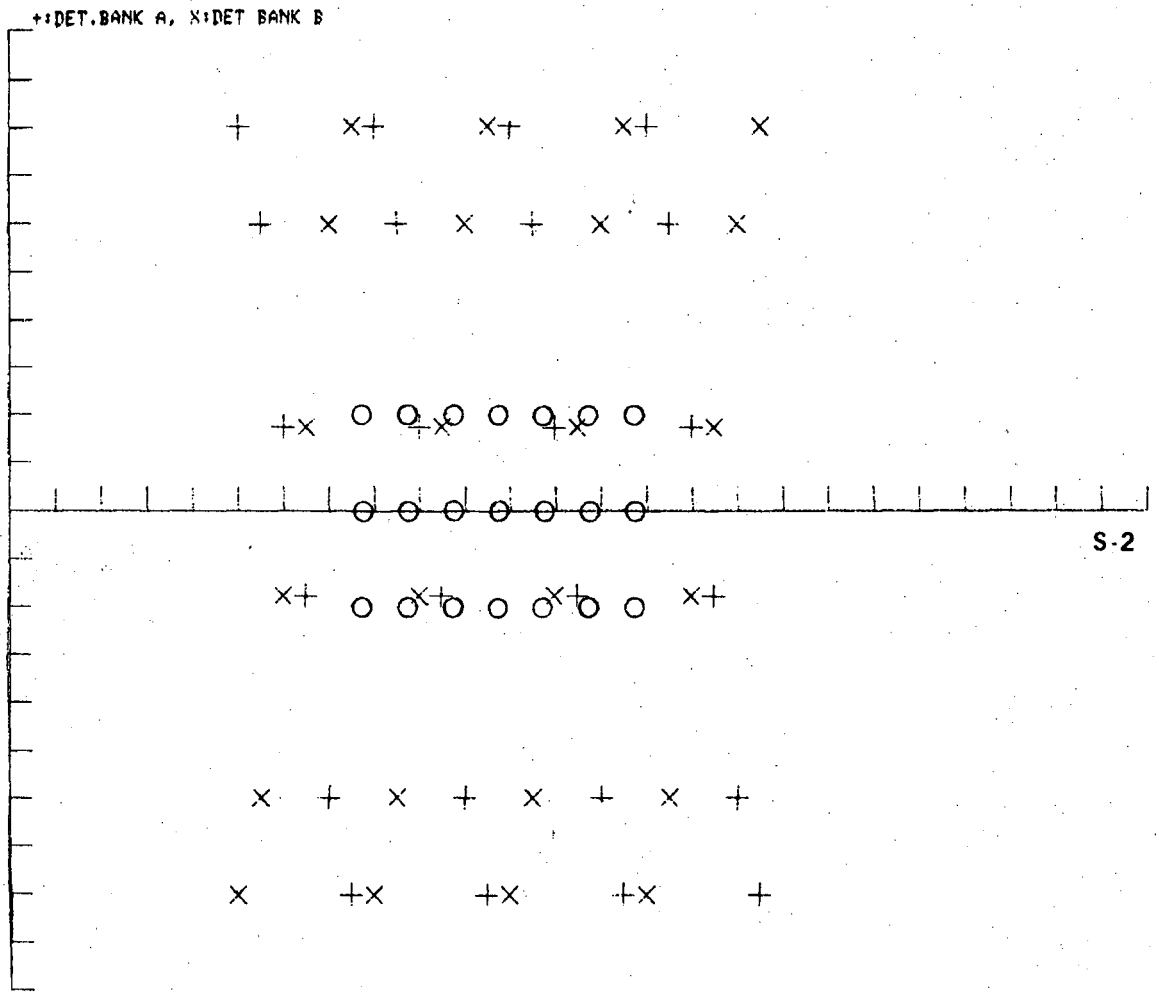

XBL 772-7751

Fig. 10

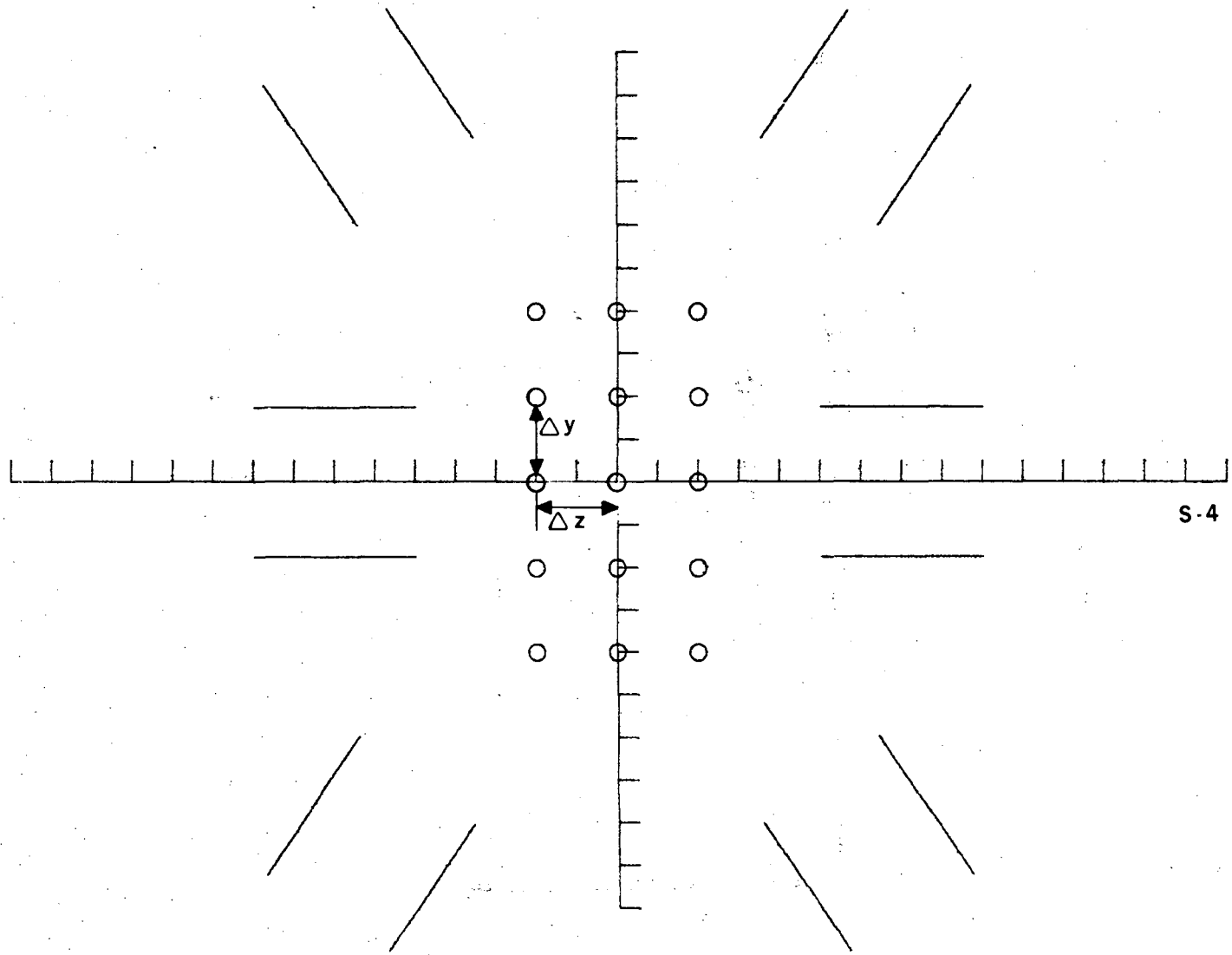

XBL 772-7727

Fig. 11

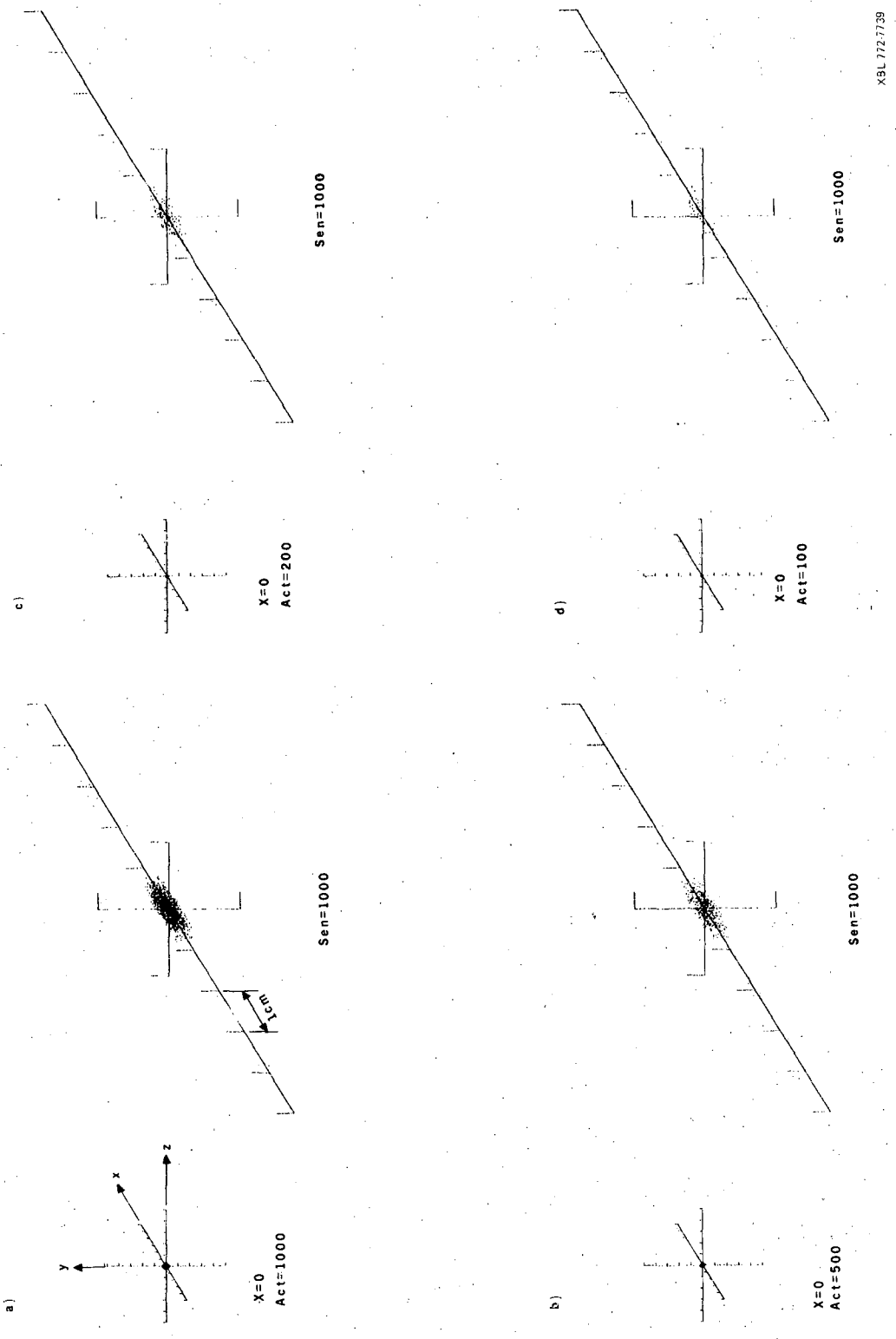

Fig. 12

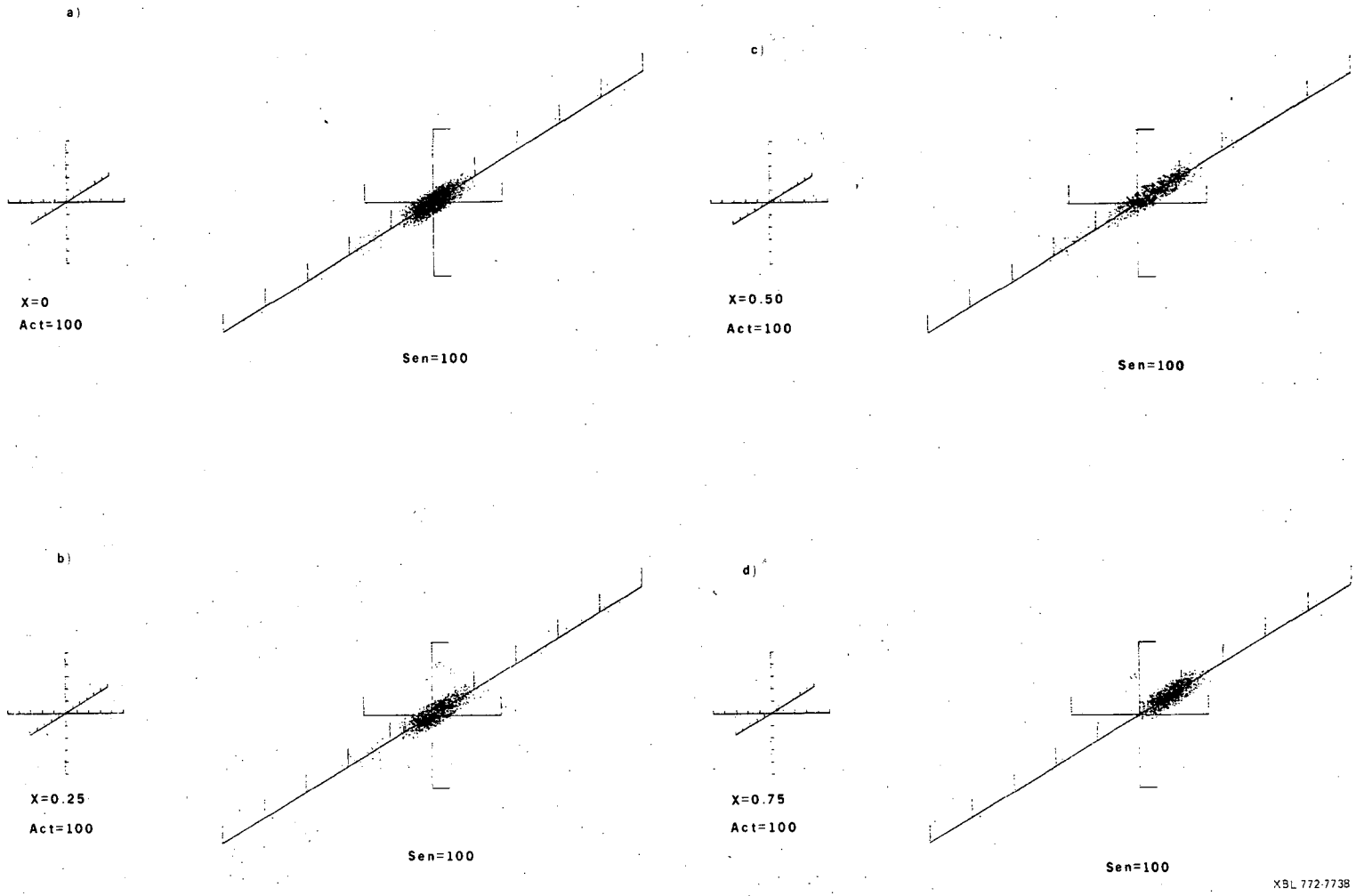
a)
X=0
Act=100
Sen=100
c)
X=0.50
Act=100
Sen=100
b)
X=0.25
Act=100
Sen=100
d)
X=0.75
Act=100
Sen=100
XBL 772-7738

Fig. 13

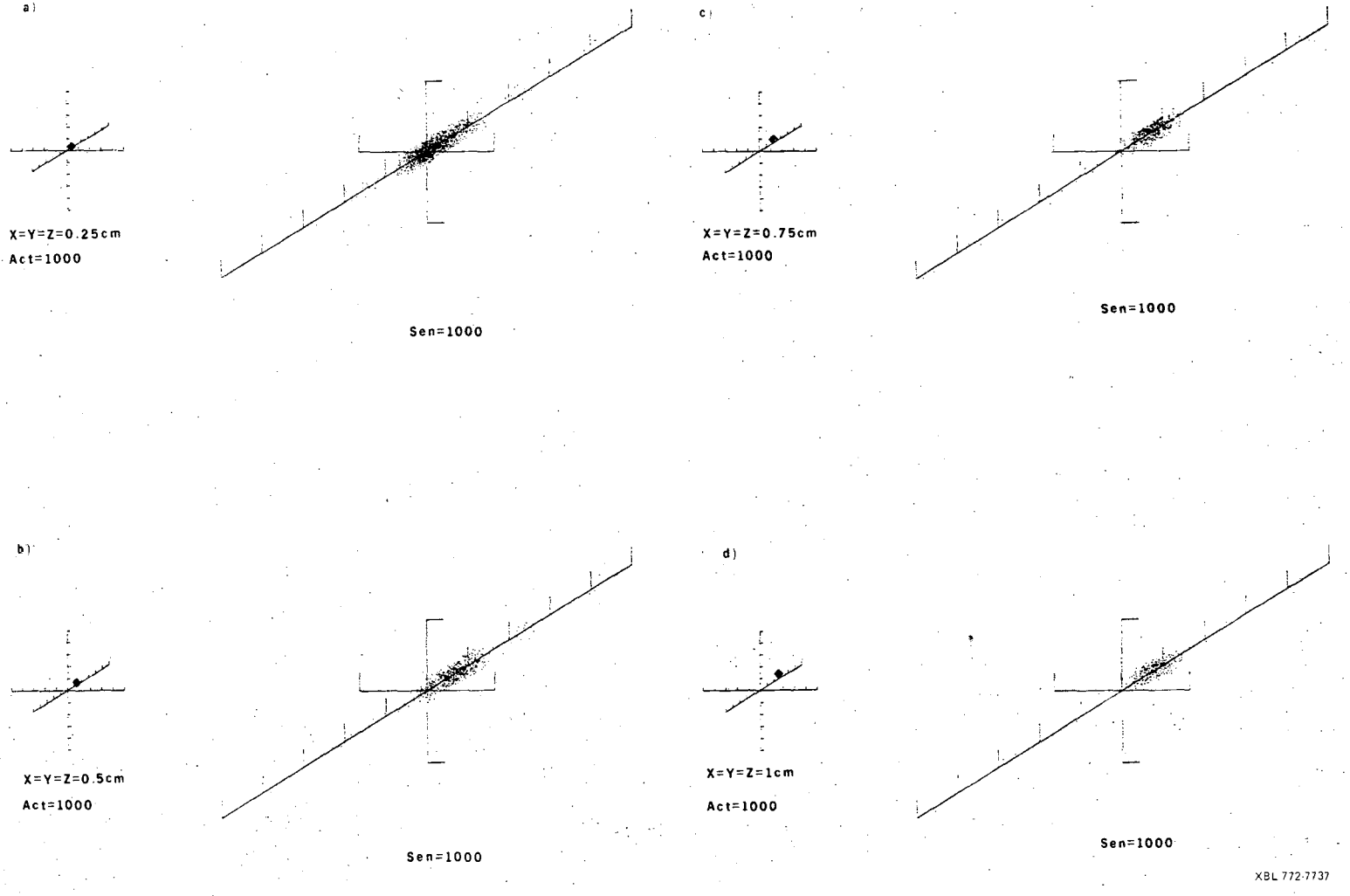

Fig. 14

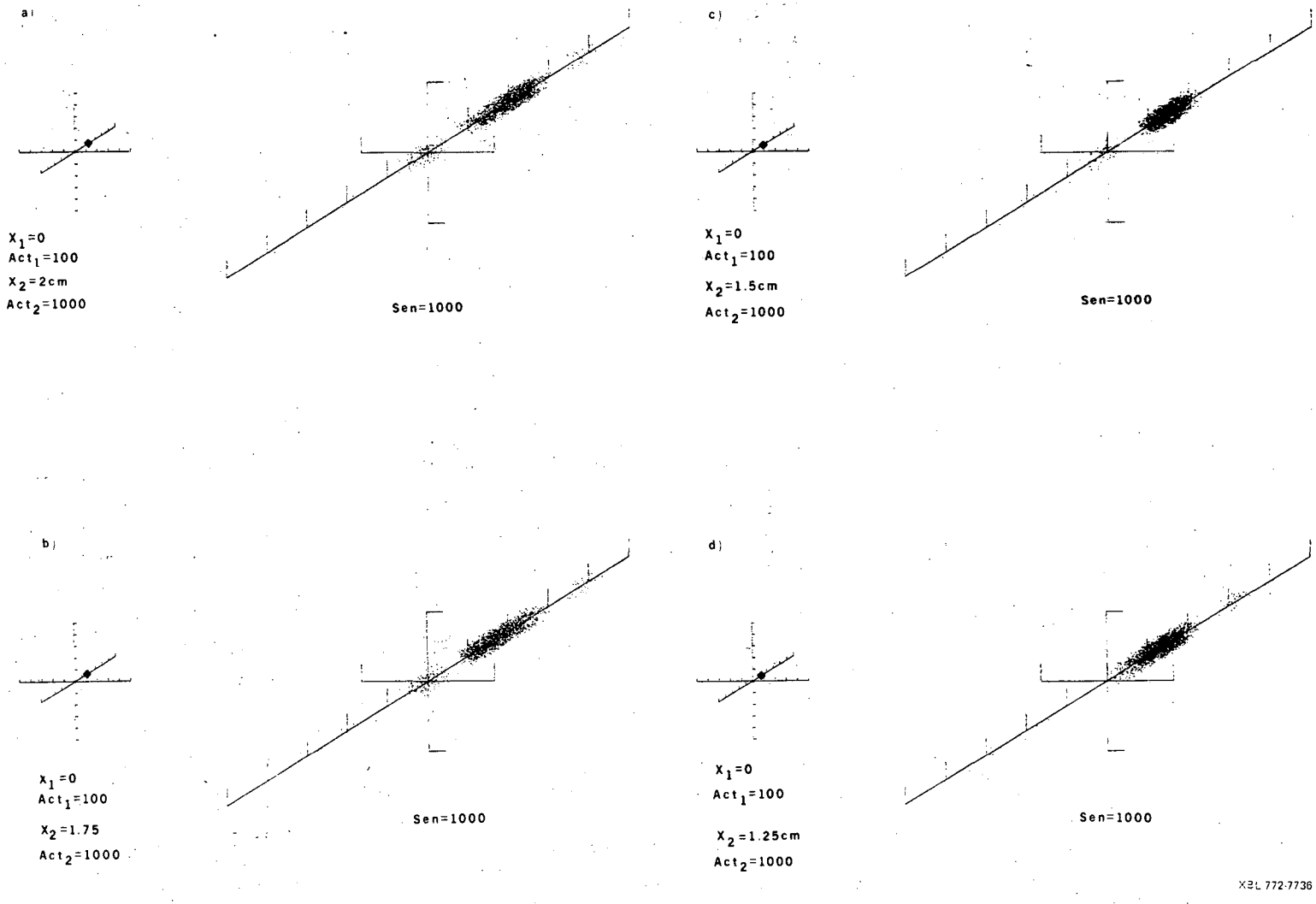
a)
X_1=0
Act_1=100
X_2=2cm
Act_2=1000
Sen=1000
c)
X_1=0
Act_1=100
X_2=1.5cm
Act_2=1000
Sen=1000
b)
X_1=0
Act_1=100
X_2=1.75
Act_2=1000
Sen=1000
d)
X_1=0
Act_1=100
X_2=1.25cm
Act_2=1000
Sen=1000
XBL 772-7736

Fig. 15

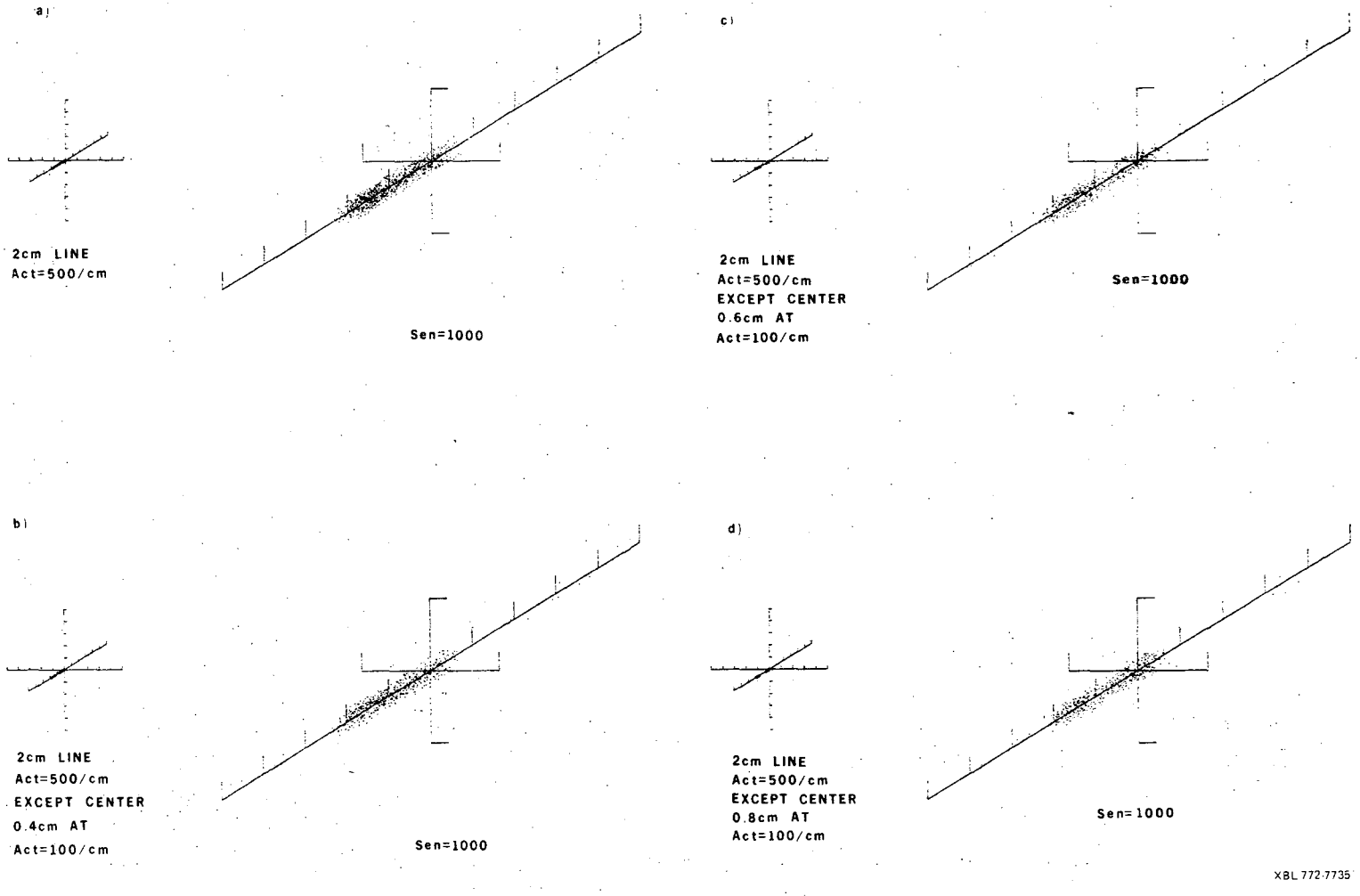

Fig. 16

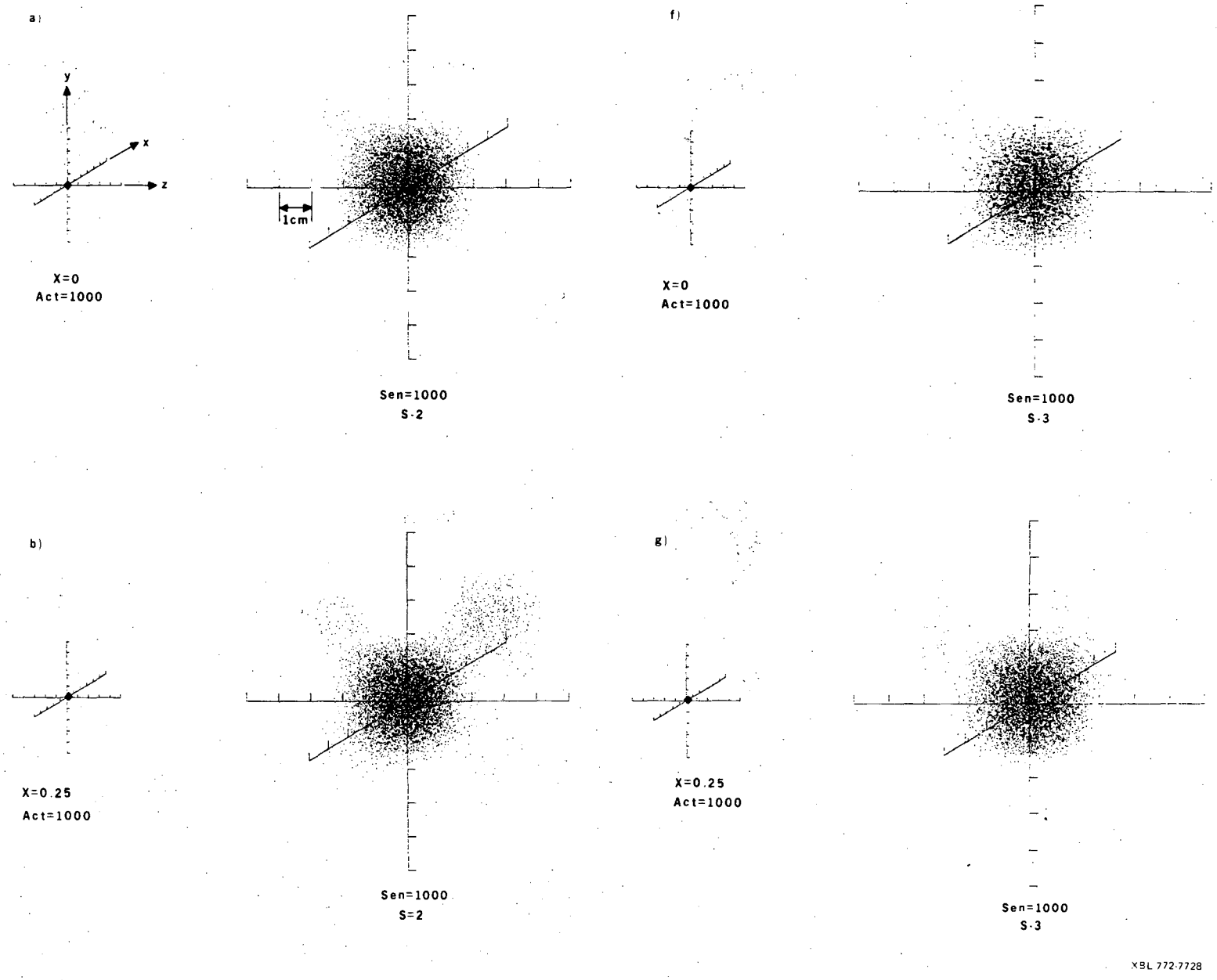
a)
y
x
z
X=0
Act=1000
1cm
Sen=1000
S-2
f)
X=0
Act=1000
Sen=1000
S-3
b)
X=0.25
Act=1000
Sen=1000
S=2
g)
X=0.25
Act=1000
Sen=1000
S-3
XBL 772-7728

Fig. 17a

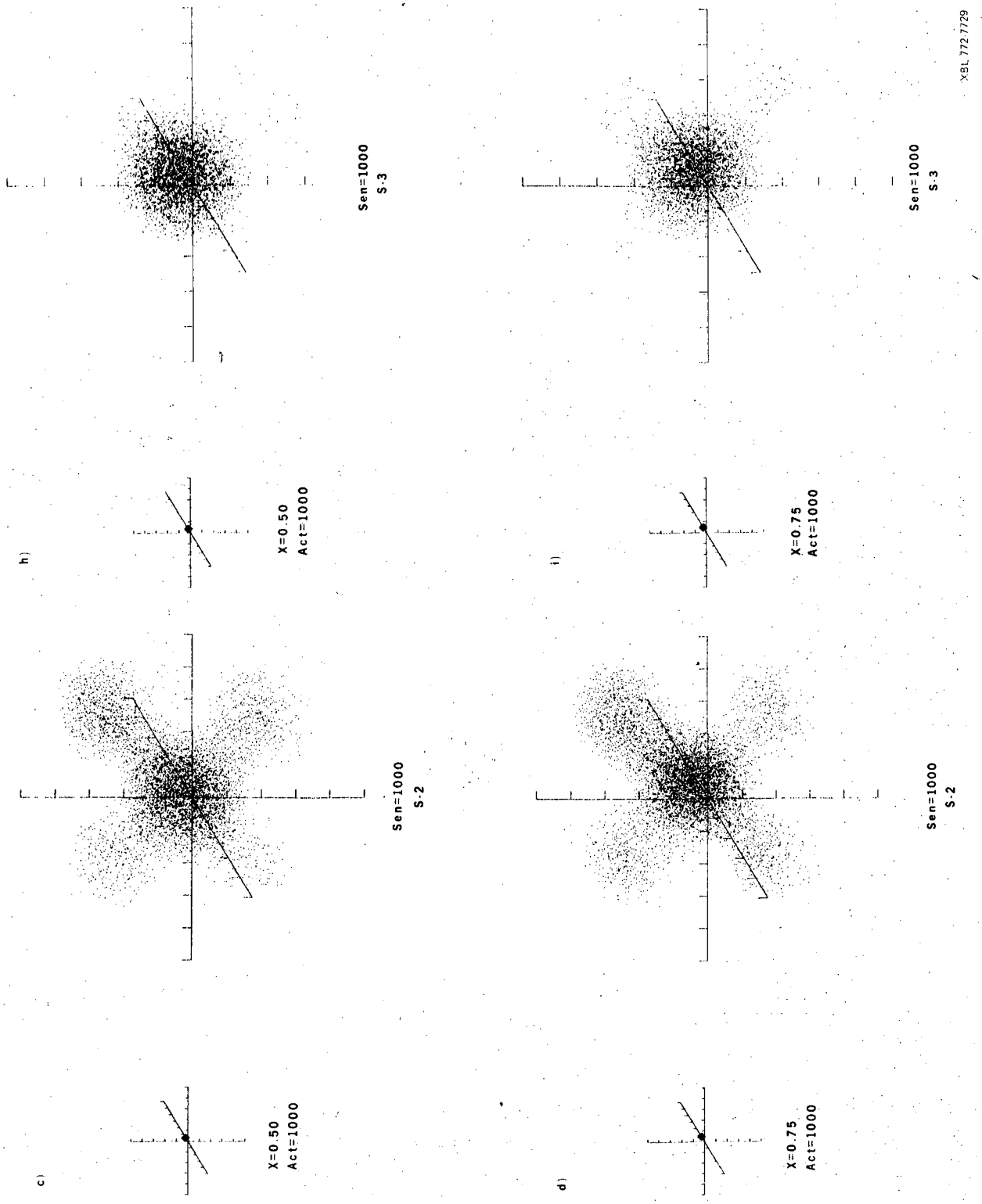

Fig. 17b

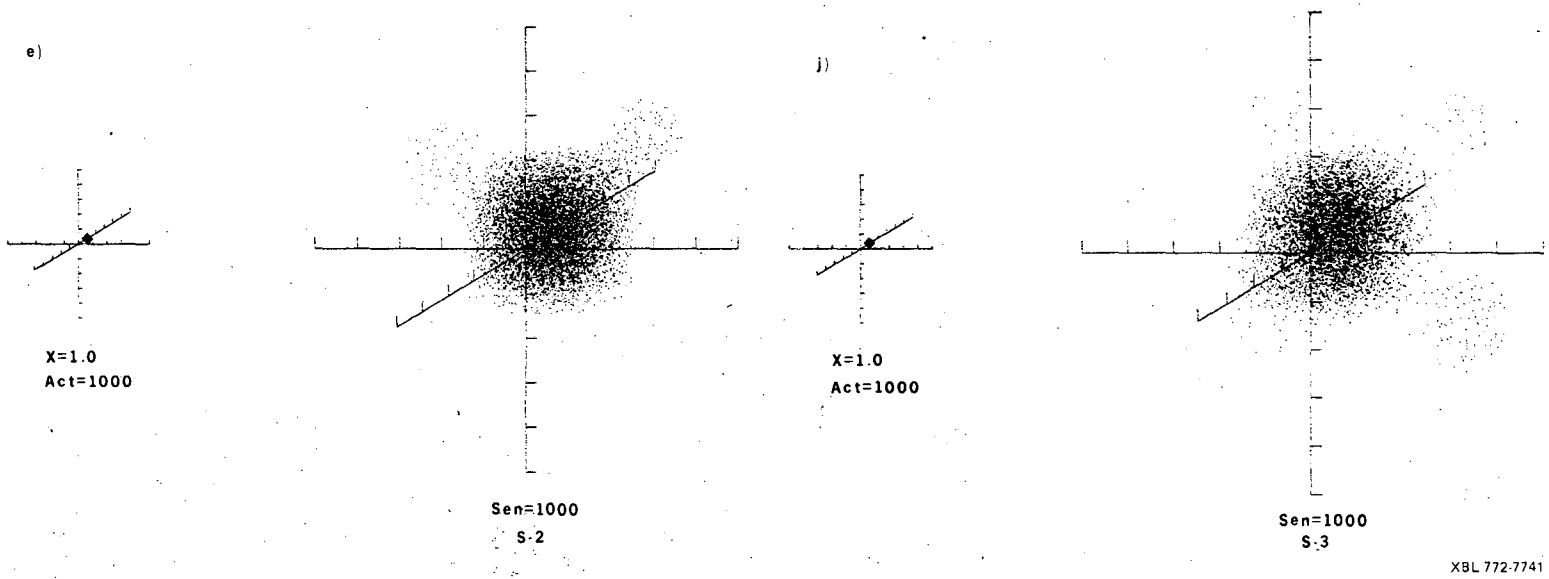
e)
X=1.0
Act=1000
Sen=1000
S-2
j)
X=1.0
Act=1000
Sen=1000
S-3
XBL 772-7741

Fig. 17c

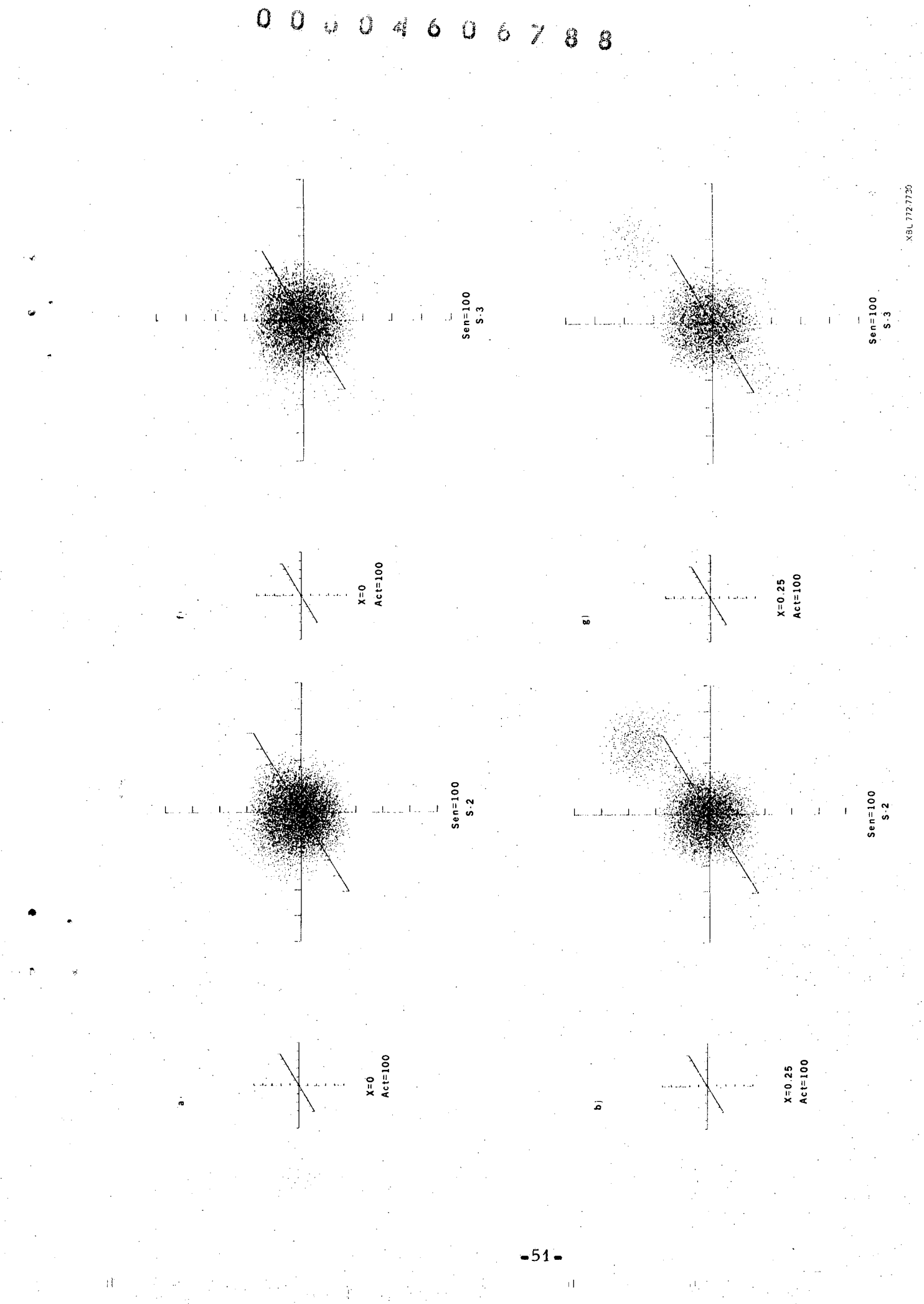

Fig. 18a

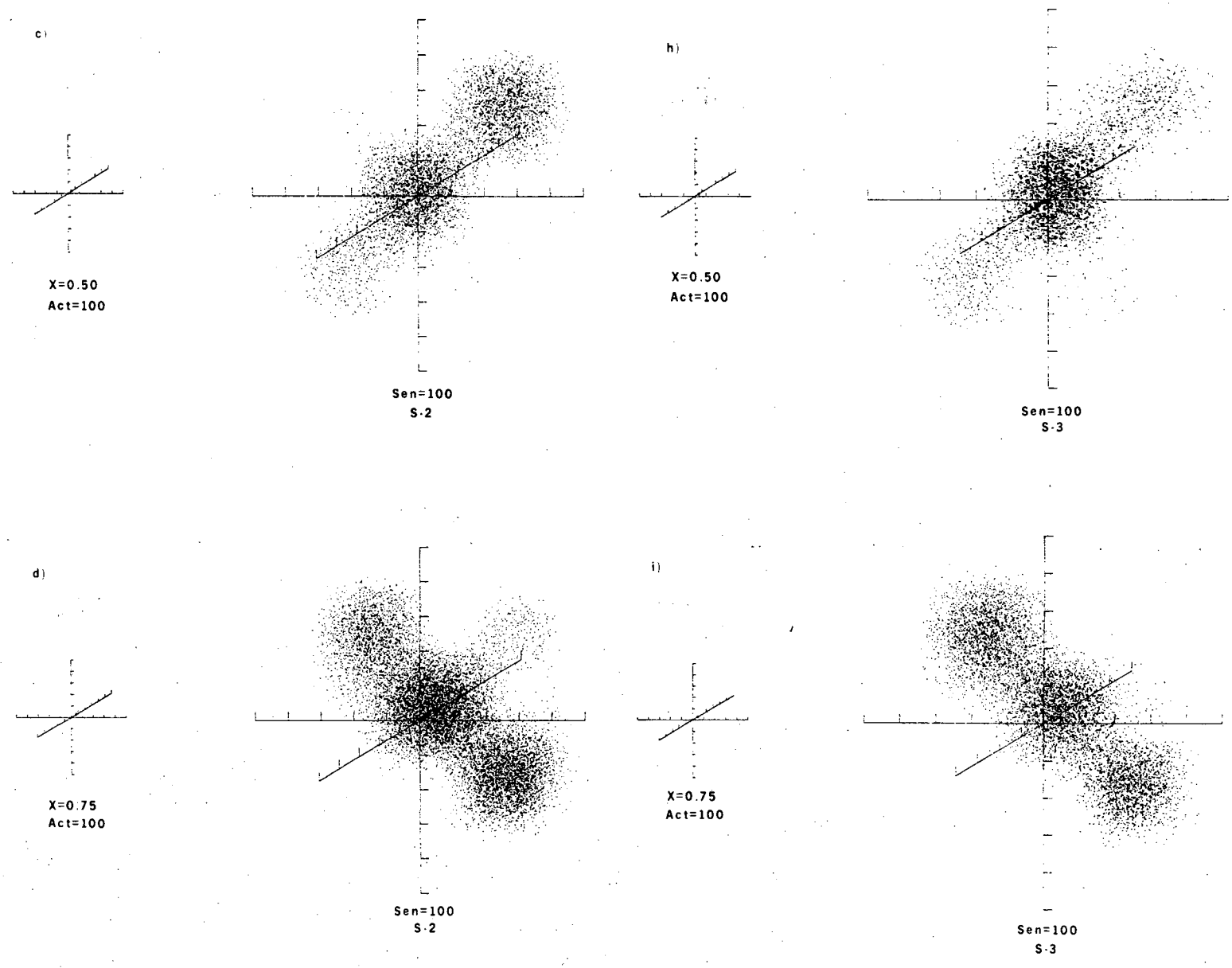
c)
X=0.50
Act=100
Sen=100
S-2
h)
X=0.50
Act=100
Sen=100
S-3
d)
X=0.75
Act=100
Sen=100
S-2
i)
X=0.75
Act=100
Sen=100
S-3
XBL 772-7731

Fig. 18b

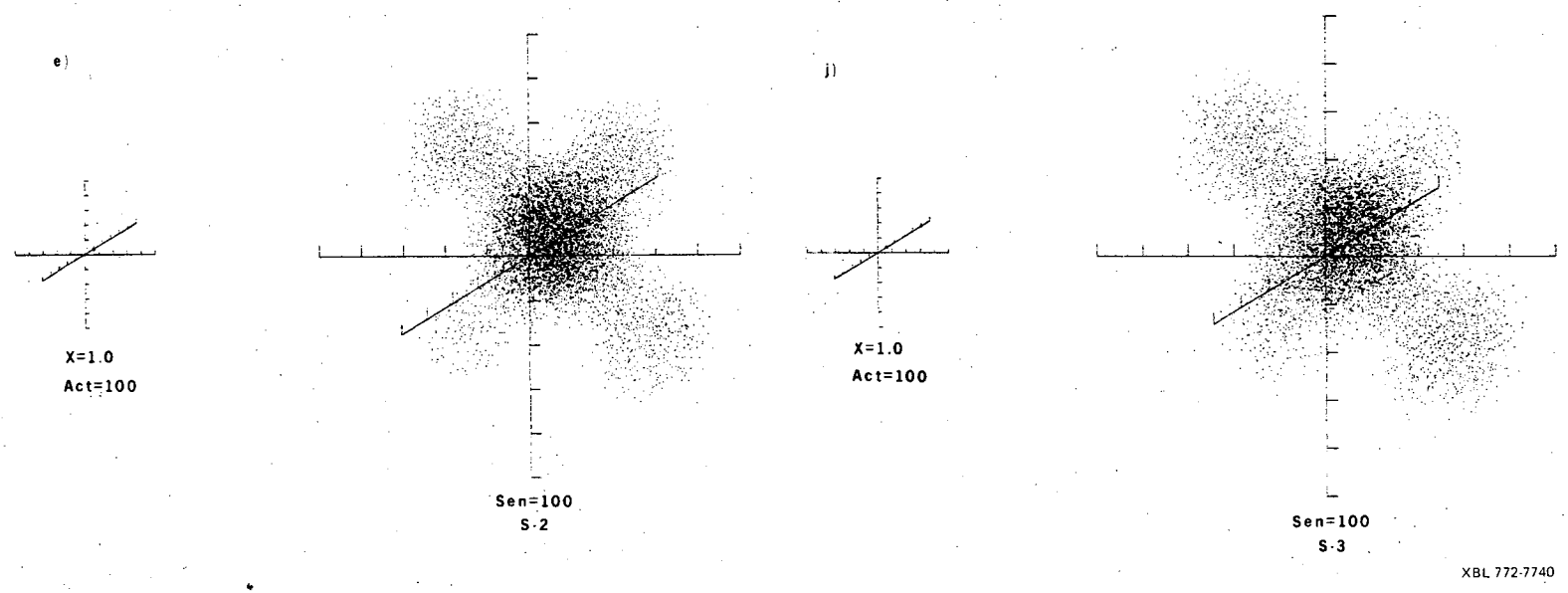

Fig. 18c

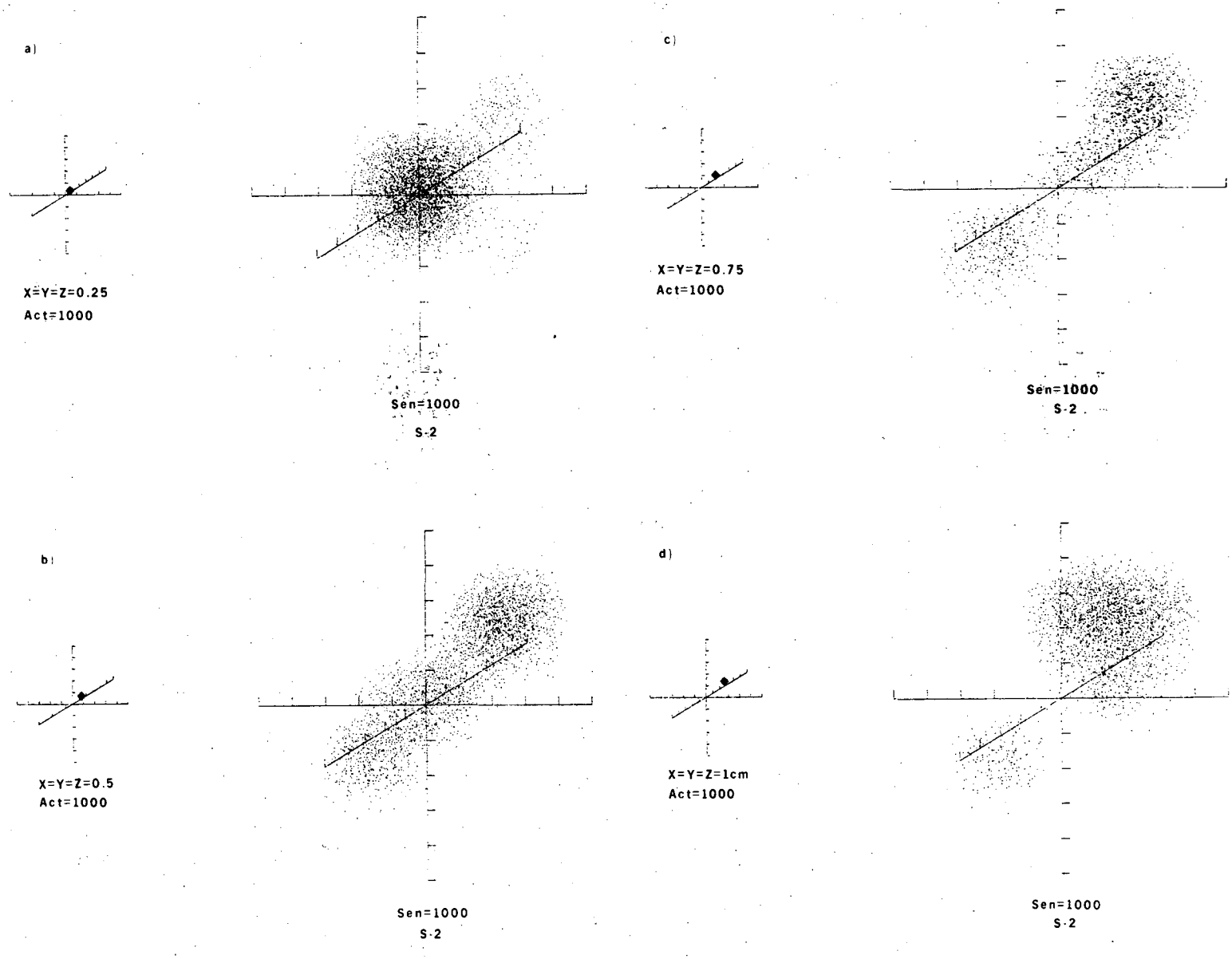
a)
X=Y=Z=0.25
Act=1000
Sen=1000
S-2
c)
X=Y=Z=0.75
Act=1000
Sen=1000
S-2
b)
X=Y=Z=0.5
Act=1000
Sen=1000
S-2
d)
X=Y=Z=1cm
Act=1000
Sen=1000
S-2
XBL 772 7732

Fig. 19a

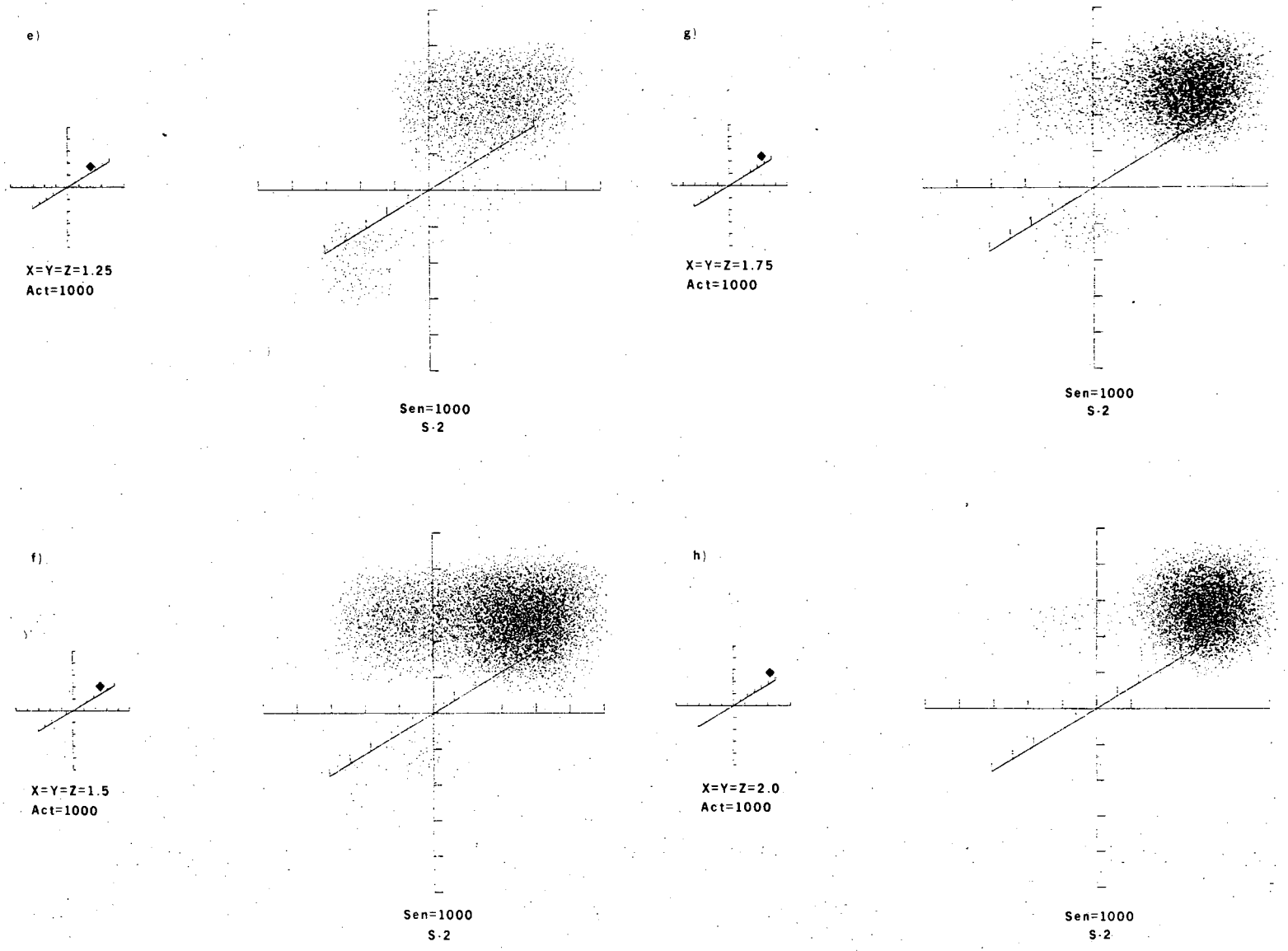

Fig. 19b

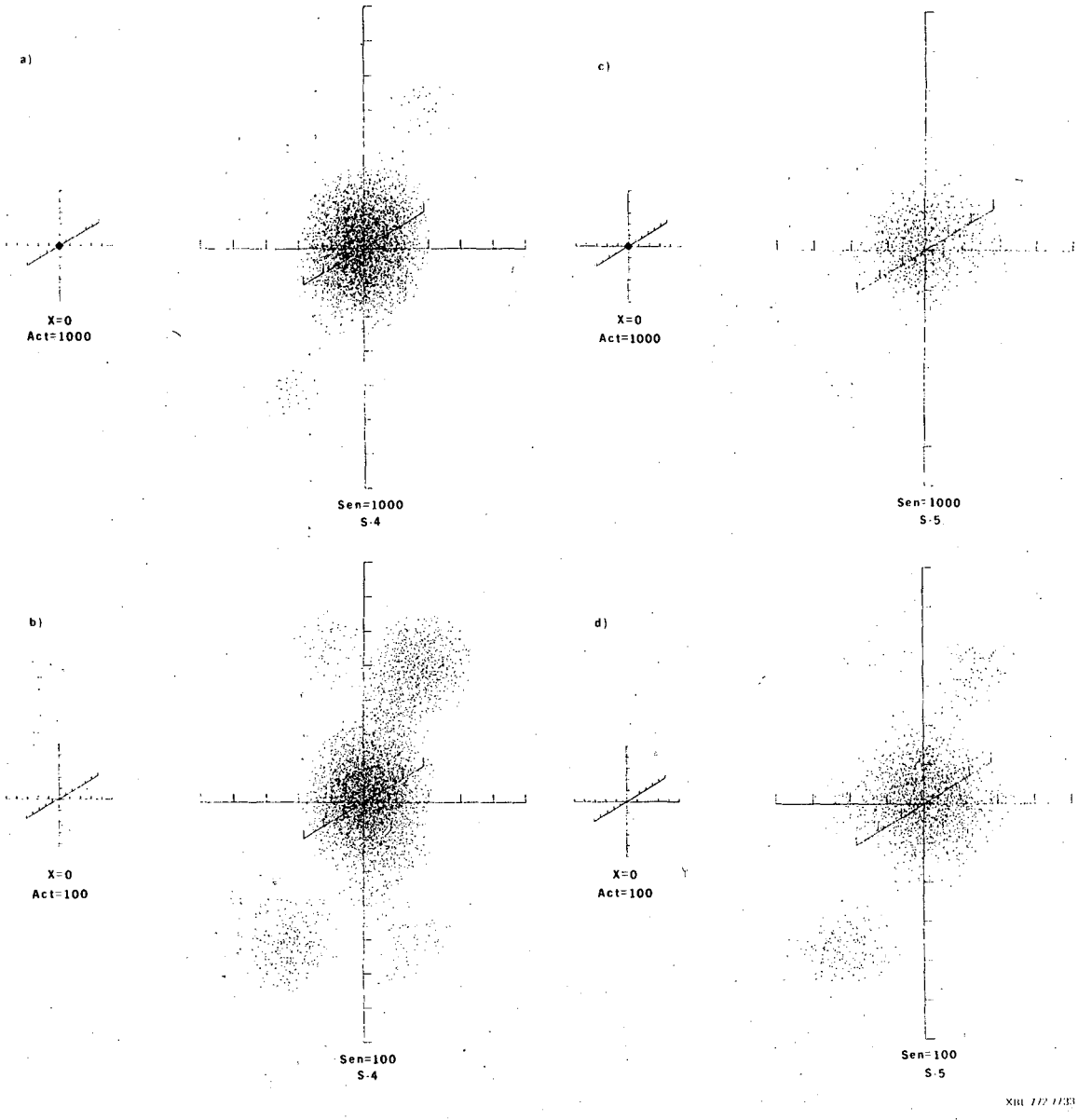
a)
X=0
Act=1000
Sen=1000
S-4
c)
X=0
Act=1000
Sen=1000
S-5
b)
X=0
Act=100
Sen=100
S-4
d)
X=0
Act=100
Sen=100
S-5

Fig. 20

This report was done with support from the United States Energy Research and Development Administration. Any conclusions or opinions expressed in this report represent solely those of the author(s) and not necessarily those of The Regents of the University of California, the Lawrence Berkeley Laboratory or the United States Energy Research and Development Administration.

TECHNICAL INFORMATION DIVISION
LAWRENCE BERKELEY LABORATORY
UNIVERSITY OF CALIFORNIA
BERKELEY, CALIFORNIA 94720